VOLUME 20, 1958/59, No. 9 pp. 245-276 Published 8th May 1959

Philips Technical Review

DEALING WITH TECHNICAL PROBLEMS
RELATING TO THE PRODUCTS, PROCESSES AND INVESTIGATIONS OF
THE PHILIPS INDUSTRIES

THE PHILIPS HOT-GAS ENGINE WITH RHOMBIC DRIVE MECHANISM

by R. J. MEIJER.

621.412-231.312

Since the first reports on the Philips hot-gas engine, published in this Review in 1946 and 1947, further research and development on the engine has taken place along two different lines. These investigations have resulted on the one hand in the construction of the cold-gas refrigerating machine, now in production for some years, and on the other hand they have led to the design of a new type of drive mechanism which is of special importance for the hot-gas engine proper (particularly large machines). By the application of this drive mechanism it has been possible to drop the idea of using one piston to perform both power and gas-transfer functions (the "double-acting" principle) and return to the thermodynamically more efficient system of separate power and transfer pistons. In this way and by the incorporation of a number of improvements in the design of regenerator, heater etc., the engine has now been given a form that promises well for future development. Measurements carried out on a 40 H.P. experimental engine built according to the new design have demonstrated that, as far as efficiency and specific power are concerned, the new engine can compete with the best amongst familiar forms of prime mover, besides possessing all the virtues inherent in the hot-gas cycle.

With the help of modern materials and with new knowledge of flow and heat-transfer phenomena, the hot-air or hot-gas cycle, which has been known since the early part of the last century, can be made to take place with high efficiency. This was made clear in a series of articles that appeared in earlier volumes of this Review [1,2,3,4,5]).

Contrary to expectation, development work on the cycle in the Philips laboratories did not in the first place lead to a hot-gas engine, but to a *gas refrigerating machine* — which, in the meantime, has come to occupy an important place in refrigeration practice [4,5]). There are several reasons for the slower development of the *engine*. The principal among these were the practical difficulties encountered when it was tried to apply what was termed the "double-acting" or single-piston principle.

This was indeed an elegant principle. The basic type of hot-gas engine, the Stirling engine, has separate power and transfer pistons, while in our "double-acting" engine one moving body performed the functions of both, this constituting a very considerable mechanical simplification. Moreover, in distinction to the small transfer-piston (or displacer-piston) engines made at the time (which worked very well), the single-piston engines did not require the crankcase to be pressurized. This promised considerable advantages for higher-power engines where a pressure crankcase would necessarily involve large-weight penalties. However, these advantages had to be paid for. In the first place an exceptionally intractable lubrication problem now arose: a piston had to act as a moving gas-tight seal between a hot and a cold space between which a large periodic pressure difference occurs. Also, both thermodynamically and aerodynamically, this type of engine was inferior to the displacer-piston engines, owing to the fact that the volume variations of the hot and cold spaces could no longer be freely chosen as regards their relative magnitude and phase.

With further development it has proved possible to drop the idea of a single "double-acting" piston and to design an engine of the *displacer-piston* type

1) H. Rinia and F. K. du Pré, Air engines, Philips tech. Rev. **8**, 129-136, 1946.
2) H. de Brey, H. Rinia and F. L. van Weenen, Fundamentals for the development of the Philips air engine, Philips tech. Rev. **9**, 97-104, 1947/48.
3) F. L. van Weenen, The construction of the Philips air engine, Philips tech. Rev. **9**, 125-134, 1947/48.
4) J. W. L. Köhler and C. O. Jonkers, Fundamentals of the gas refrigerating machine, Philips tech. Rev. **16**, 69-78, 1954/55.
5) J. W. L. Köhler and C. O. Jonkers, Construction of a gas refrigerating machine, Philips tech. Rev. **16**, 105-115, 1954/55.

which also possesses the feature that the crankcase need not be pressurized. This was made possible by the embodiment of a new kind of drive mechanism. The latter offers the additional advantage that even a one-cylinder engine can be perfectly balanced. Of the various engines built according to this design, a single-cylinder 40 H.P. machine will be described here and some results of measurements of the output and efficiency will be given.

To save the reader the trouble of consulting earlier volumes of this Review, we shall now very briefly recapitulate the principles of the hot-gas engine, restricting ourselves to an engine provided with a displacer piston.

Brief account of the hot-gas cycle

An internal-combustion engine provides a surplus of work in virtue of the compression at low temperature of a certain quantity of air, to which atomized fuel is added either before or after the compression, the subsequent heating of the mixture by rapid combustion, and its expansion at high temperature.

The hot-gas engine is based on the same principle, i.e. the compression at low temperature and expansion at high temperature of a given quantity of gas. The heating takes place, however, in an entirely different manner, the heat being supplied to the gas from outside, through a wall. For this reason the description "external-combustion engine" is appropriate. Owing to the high thermal capacity of the wall, it is not of course possible to heat and cool the gas simply by rapid heating and cooling of the wall. Stirling had realized as far back as 1817, however, that the gas temperature could be made to change periodically by causing a "displacer piston" to transfer the gas back and forth between two spaces, one at a fixed high temperature and the other at a fixed low temperature — see *fig. 1*. If we raise the displacer piston in fig. 1, the gas will flow from the hot space via the heater and cooler ducts into the cold space. If now the displacer piston is moved downwards the gas will return to the hot space along the same path. During the first transfer stroke the gas has to yield up a large quantity of heat; an equal quantity of heat has to be taken up during the second stroke. The *regenerator* shown in fig. 1 is inserted between the heater duct and cooler duct in order to prevent unnecessary wastage of this heat. It is a space filled with porous material to which the hot gas yields heat before entering the cooler; when the gas streams back, it takes up the stored heat again prior to its entry into the heater.

The displacer system, which serves to heat and cool the gas periodically, is combined with a power piston that compresses the gas while it is in the cold space and allows it to expand while in the hot space (all dead spaces in cooler, heater etc. being disregarded). Since compression takes place at a lower temperature than expansion, a surplus of work results. *Fig. 2* shows four phases of the cycle through which the whole system passes if a *discontinuous* movement of power piston and displacer piston is presupposed. The displacements they are assumed to undergo are plotted as functions of time in *fig. 3*; the ordinates in band *E* represent the variation in the volume of the hot space, and those in band *C* the variation in the volume of the cold space. The volume variations are plotted separately in the lower part of the diagram. *Fig. 4* is the p,V diagram of the cycle (V is the total volume of the gas).

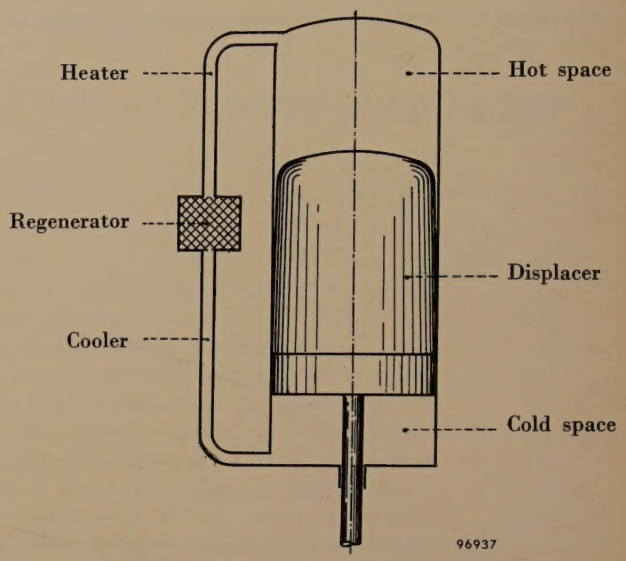

Fig. 1. Principle of the displacer-piston system. Moving this piston up and down causes the gas to be transferred back and forth between the hot and cold spaces, via heater, regenerator and cooler.

In a practical version of the engine the movements of power and displacer pistons must of course be *continuous*, not discontinuous, as they have been assumed to be in these figures; the continuous movements will be obtained with the aid of some kind of crank and connecting rod mechanism. It will not then be possible to distinguish any sharp transitions between the four phases, but this will not alter the principle of the cycle (or detract from its efficiency — see below). The movements of power piston and displacer might now be as indicated in *fig. 5*, in which the volume variations of the cold and hot spaces have again been plotted separately. The only essential condition for obtaining a surplus of work is that the volume variation of the hot space should

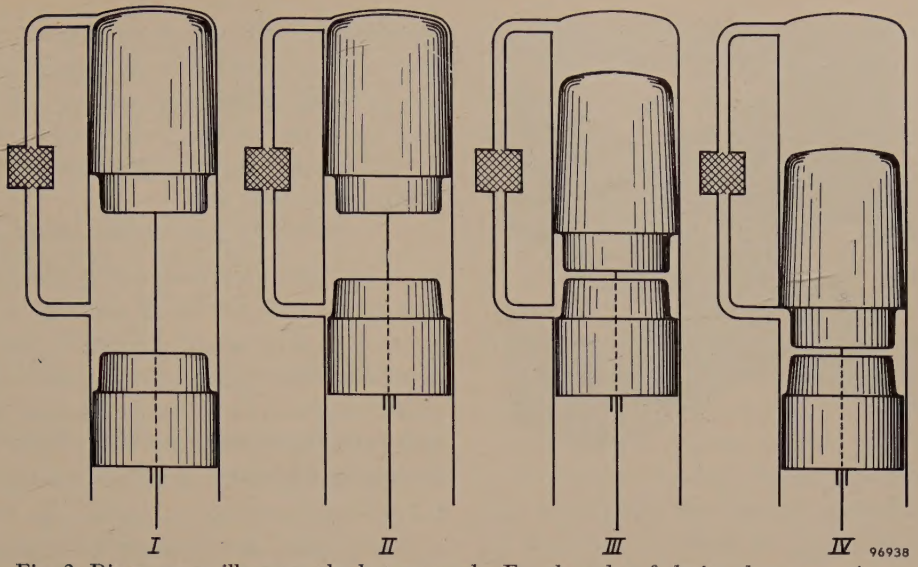

Fig. 2. Diagrams to illustrate the hot-gas cycle. For the sake of clarity the power piston and the displacer piston are supposed to move discontinuously; it is then possible to distinguish four phases that make up the complete cycle.

I Power piston is in lowest, displacer piston in highest position. All the gas is in the cold space.

II The displacer piston is still in the highest position. The power piston has compressed the gas while it is at low temperature.

III The power piston is still in its highest position. The displacer piston has pushed the gas through the cooler, regenerator and heater into the hot space.

IV The hot gas has expanded, and the power and displacer pistons have together returned to the lowest position. While the power piston remains there, the displacer piston will now push the gas through heater, regenerator and cooler into the cold space, whereupon situation *I* will have been restored.

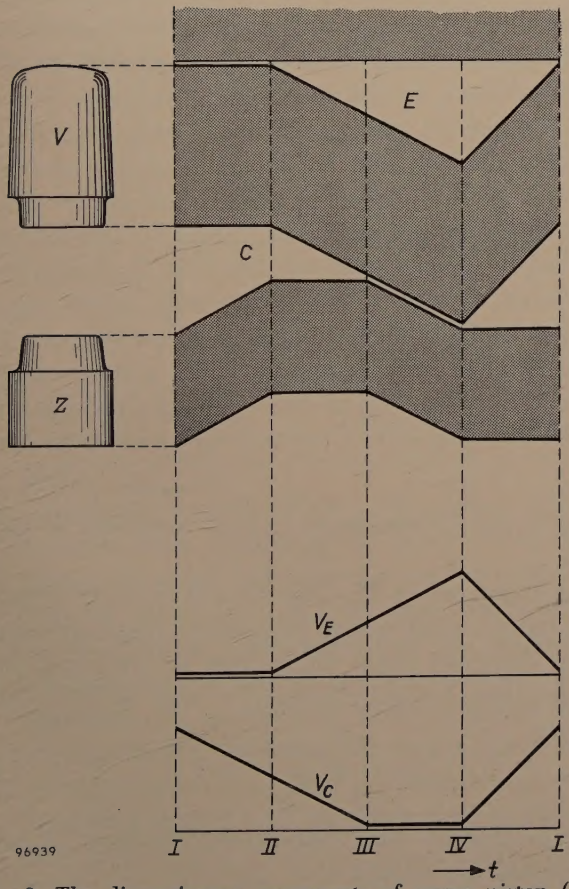

Fig. 3. The discontinuous movements of power piston (Z) and displacer piston (V) assumed in fig. 2, plotted as functions of the time. Band E represents the volume variatons of the hot space, band C those of the cold space. These variations are plotted separately lower in the diagram.

have a phase lead with respect to that of the cold space; this is equivalent to requiring that the appropriate p,V diagram, shown in *fig. 6*, should be traced out in the clockwise direction.

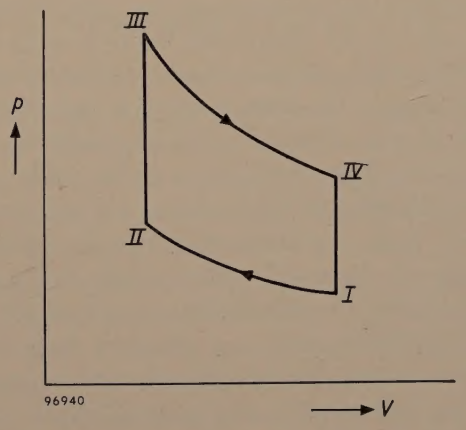

Fig. 4. The p,V diagram of the hot-gas cycle represented by fig. 3.

For the subsequent discussion of specific power and efficiency it will be necessary to recall the more important of the formulae worked out in the articles cited. They are based on the assumption that V_E, the volume of the hot (expansion) space, and V_C, the volume of the cold (compression) space, vary with the crank angle α in a purely sinusoidal fashion:

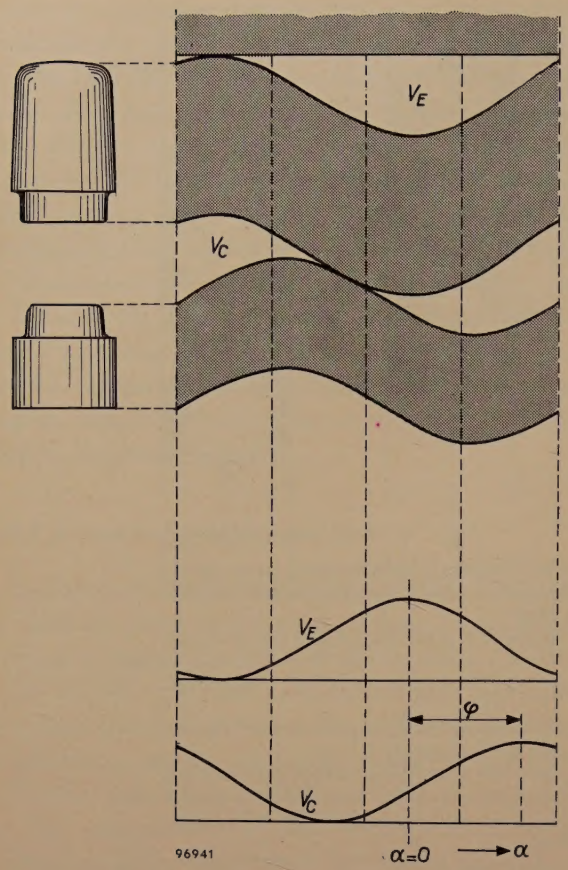

Fig. 5. As for fig. 3, except that now the piston and displacer movements are *continuous* (the abscissa represents the crank angle α). It is no longer possible to distinguish sharp transitions between the phases of the cycle.

$$\left.\begin{aligned} V_E &= \tfrac{1}{2}V_0(1+\cos\alpha),\\ V_C &= \tfrac{1}{2}wV_0[1+\cos(\alpha-\varphi)]. \end{aligned}\right\} \quad . \; . \quad (1)$$

The crank angle α (for constant angular velocity ω, proportional to the time: $\alpha = \omega t$) is measured from the position at which V_E has its maximum value V_0; φ is the phase angle between the volume variations of the hot and cold spaces, and w is the ratio between their maximum volumes. In reality the variations in V_E and V_C will certainly not be purely sinusoidal, but the calculations show that the effect of the higher harmonics can generally be neglected. A further assumption underlies the derivation of the formulae, namely that the cycle is "ideal", characterized by constant gas temperatures T_E and T_C in the hot and cold spaces respectively, and negligible flow and other losses (to which we shall return later on). Another important quantity introduced is the gas temperature ratio,

$$\tau = T_C/T_E \qquad (\tau < 1). \; . \; . \; . \quad (2)$$

The condition that the mass of the working fluid remains constant throughout the cycle now leads to the formula for the pressure p as a function of the crank angle:

$$p = p_{max}\frac{1-\delta}{1+\delta\cos(\alpha-\Theta)}, \quad . \; . \; . \quad (3)$$

in which p_{max} is the maximum pressure occurring during the cycle and

$$\delta = \frac{\sqrt{\tau^2 + w^2 + 2\tau w\cos\varphi}}{\tau + w + 2s}, \quad . \; . \; . \quad (4)$$

$$\tan\Theta = \frac{w\sin\varphi}{\tau + w\cos\varphi} \qquad (\Theta < 180°) \; . \quad (5)$$

(s is the relative volume of the "reduced dead space"). From the above we obtain the average pressure,

$$\bar{p} = p_{max}\sqrt{\frac{1-\delta}{1+\delta}}, \; . \; . \; . \; . \; . \quad (6)$$

and the power output

$$P = \tfrac{1}{2}\omega V_0\bar{p}\,(1-\tau)\frac{\delta}{1+\sqrt{1-\delta^2}}\sin\Theta. \; . \; . \quad (7)$$

We are concerned here with a reversible cyclic process in which, in accordance with the "idealized" conditions assumed (isothermal behaviour in cold and hot spaces and 100% efficient regenerator action), the supply of heat takes place at only one temperature T_E and the removal of heat at only one temperature T_C. There is a theorem in thermodynamics which states that under these conditions the efficiency with which heat is converted into work (the thermal efficiency) is that of the Carnot cycle:

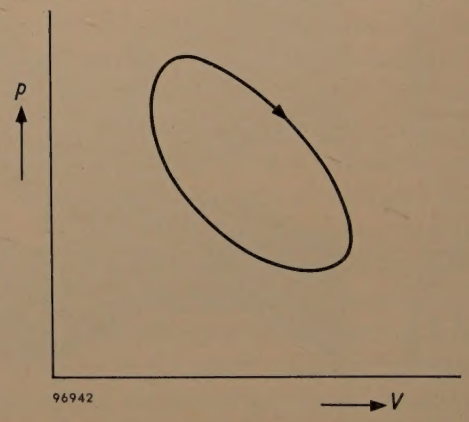

Fig. 6. The p,V diagram of the cycle represented by fig. 5.

$$\eta = \frac{T_E - T_C}{T_E} = 1-\tau. \; . \; . \; . \quad (8)$$

From this we may obtain the quantity of heat supplied per second,

$$q_E = \frac{P}{\eta} = \tfrac{1}{2}\omega V_0\bar{p}\frac{\delta}{1+\sqrt{1-\delta^2}}\sin\Theta. \; . \quad (9)$$

This recapitulation will suffice for our present purposes. We shall now go on to draw certain conclusions which have been essential in deciding the manner in which the cycle must be made to take place in a practical hot-gas engine.

Specific power, losses and overall efficiency

The main considerations governing the design of an engine will in general be to see that its specific power and overall efficiency are as high as possible (consistent, of course, with certain conditions, such as a reasonable working life). The former term refers to the power output per unit volume swept out by the power piston. Overall efficiency is defined as the ratio of work performed per unit time divided by the heat content of the fuel consumed per unit time. These two aims are in some respects contradictory.

We see from formula (7) that the output of a given engine (for which certain values of the parameters w, φ and s have been decided upon) can be stepped up by increasing the mean pressure $\bar{p}$ and the shaft revolutions n (angular velocity ω) and by reducing the ratio τ. A reduction in τ also brings about a direct improvement in the efficiency; formula (8) shows that, theoretically, η is dependent on τ alone. The coolant temperature, which determines T_C, should therefore be made as low as possible, and the temperature T_E at which heat is supplied to the heater element should be made as high as possible, i.e. as high as the properties of the heater wall material (e.g. resistance to creep and oxidation) will permit. To find out the effect on the efficiency, if any, of the other two factors, $\bar{p}$ and n, we shall have to pay attention to the various kinds of *losses*, which are not taken account of the in formulae. The following are the most important [6]).

a) Losses due to mechanical friction in the moving parts.

b) "Adiabatic losses". Within the spaces whose volumes vary, expansion and compression take place more or less adiabatically, not isothermally, with the result that T_{Ea}, the mean temperature in the hot space, will be lower than T_E, the heater temperature and that at which heat is supplied. Similarly, T_{Ca} in the cold space is higher than T_C. Internally, therefore, the engine has a temperature ratio $\tau_a = T_{Ca}/T_{Ea}$ which is greater than the external τ, the implication being a lower efficiency.

c) Fluid friction or flow losses, representing the work done in forcing the gas to flow back and forth through cooler, regenerator and heater.

d) Regenerator losses. Since in practice a regenerator can never be 100% effective, the temperature of the gas leaving it is too high on entry into the cooler and too low on entry into the heater. Thus an additional amount of heat is removed in the cooler, and lost to the engine.

e) Heat-transfer losses at the walls of the elements responsible for heat exchange between the working fluid on the one hand and the coolant and combustion gases on the other. As with the "adiabatic losses", these losses have the consequence that the ratio τ is effectively increased.

f) Flue losses, which are inevitable in any kind of burner. The hot burning gases can yield up heat to the heater body only while their temperature is yet above that of the latter. When they have cooled to this temperature the remaining heat content of the gases will — if no special measures are taken — be lost via the flue. These flue losses can, however, be considerably reduced by further cooling the flue gases by heat exchange with the incoming fresh air, which is consequently preheated.

Now, closer consideration of the influence of $\bar{p}$ and n on the losses shows that the former factor has little effect on their relative magnitude [7]). Hence it is always advantageous to make $\bar{p}$ as high as possible; the experimental engine that will be described below was designed for an average pressure $\bar{p}$ of up to about 100 kg/cm². On the other hand, an increase in the engine speed does affect efficiency adversely, because the *flow losses* increase with n at more than a strictly proportional rate. These losses, however, do not only depend on the engine speed (and, of course, on the dimensioning of the ducts); they differ considerably according to the gas used as the working fluid. Since the hot-gas cycle takes place within a closed system, the designer has a free choice as to the gas so used. We decided on *hydrogen* as the working fluid for the new engine. Owing to its low density, flow losses are not excessive even at considerable engine speeds. Moreover, with hydrogen good heat-transfer characteristics are attainable. In the machine described here the nominal running speed is 1500 r.p.m.

---

[6]) Losses (*a*) to (*e*) inclusive were discussed at rather greater length with reference to the cold-gas refrigerating machine [5]), in which they likewise occur; the losses under (*f*) are of course absent in the refrigerating machine.

[7]) However, the relative magnitude of the losses (*e*) does depend somewhat on the power developed by the engine and therefore also on $\bar{p}$ (and n too): the greater the rate at which it is desired to pass heat through a given area of heat-exchanger wall, the greater will be the temperature drop across the wall, and hence the smaller is the internal temperature difference, i.e. the greater is the ratio τ.

Helium may also be used as the working fluid instead of hydrogen. The overall efficiency is then found to be somewhat lower.

The further details of the engine we shall now proceed to describe are mainly concerned with the new drive mechanism to which reference has already been made, the design of regenerator, heater, cooler and air pre-heater and finally a complete control system for regulating the power of the engine.

The drive mechanism of the displacer-piston machine

Earlier versions

There are various ways of making the power and displacer pistons perform the required movements. *Fig. 7* shows a drive mechanism of a kind that used to be embodied in small hot-gas engines. The power piston is linked to the crankshaft K by a connecting rod (con-rod) D in the normal way; the movement of the displacer is derived from that of the power piston with the aid of the rocker T, which is linked by arm S_1 to the displacer-piston rod V and by arm S_2 to a certain point on the power-piston con-rod. The latter has to be forked in order to leave free passage for the arm S_1 and the displacer-piston rod, which passes centrally through the power piston. A different form of drive mechanism has been adopted for the Philips gas refrigerating machine — see *fig. 8*. There are three cranks in the shaft, and the two outside ones, which lie at the same angle, are linked to the piston by two parallel con-rods; the displacer piston is actuated from the middle crank, which is offset by a certain angle from the other two.

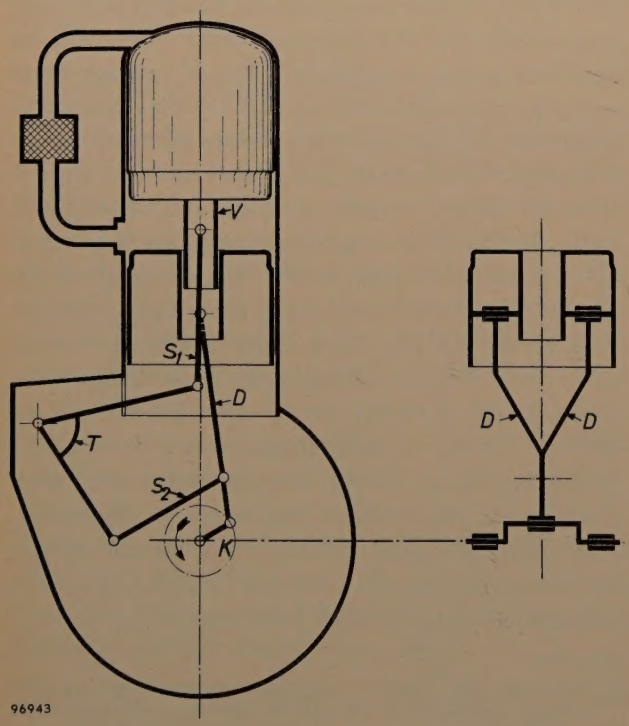

Fig. 7. Drive mechanism of the kind formerly used in small hot-gas engines. D = forked piston con-rod. K = crankshaft. T = rocker linked by arms S_1 and S_2 to the displacer-piston rod V and to a certain point on D.

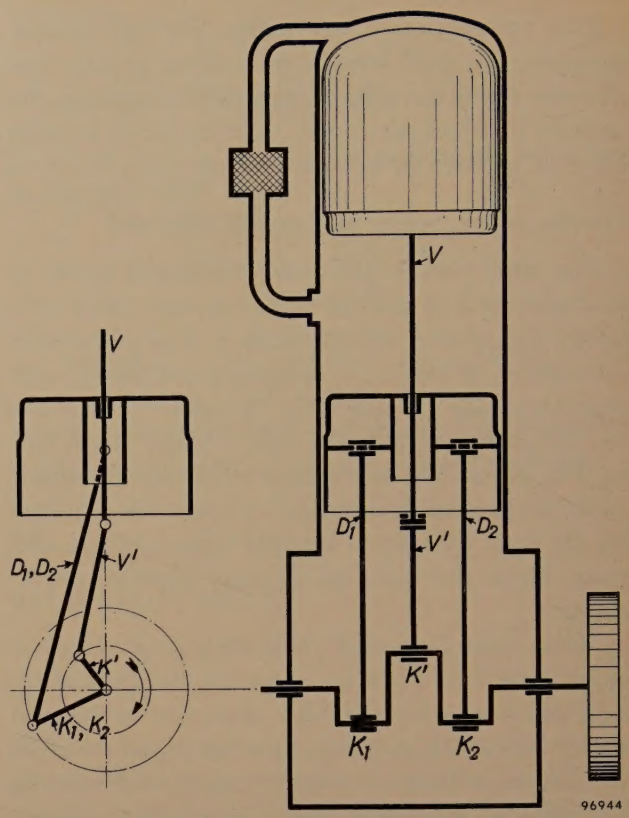

Fig. 8. Drive mechanism used in the gas refrigerating machine. The piston has two parallel con-rods D_1 and D_2 which link it to cranks K_1 and K_2; between the latter is a third crank K', which con-rod V' links to the displacer-piston rod V.

We alluded in the introduction to the drawback of mechanisms such as those of figs. 7 and 8, especially for large engines: the crankcase has to be filled with the working gas under high pressure. This is necessary for two reasons: first, to limit the leakage of gas past the piston; second, to preclude unnecessarily large downward forces on the drive mechanism. In the absence of any compensating pressure (buffer pressure) in the crankcase there is a difference of pressure across the piston fluctuating between p_{min} and p_{max}, the minimum and maximum pressures occurring within the cylinder during the cycle. Introducing a buffer pressure of value p_{min}, for example, reduces the maximum pressure difference across the piston to $p_{max} - p_{min}$.

It is clear that with such a pressurized crankcase considerable weight penalties are involved. Particularly troublesome in large engines, this drawback becomes even more of an embarrassment if it is

desired to operate at very high pressures in order to increase the specific power in the way explained above.

The new drive mechanism (rhombic drive)

The above-mentioned drawbacks do not arise in the new drive, which we now propose to describe. Briefly, it comprises twin cranks and con-rod mechanisms, identical in design and offset from the central axis of the engine; the cranks rotate in opposite senses and are coupled by two gearwheels.

Fig. 9 is a schematic diagram of the system. Fixed to the power piston *1* by way of piston rod *2* is a yoke *3*. One end of the yoke is linked by con-rod *4* to crank *5*, the other end by con-rod *4'* to crank *5'*. The displacer piston is actuated by a precisely similar arrangement: the displacer-piston rod *7*, which passes through the hollow rod *2*, has fixed to it a yoke *8* which is linked to cranks *5* and *5'* by con-rods *9* and *9'* respectively. If *9* and *9'* are given the same length as *4* and *4'*, the two pairs of con-rods will form a rhombus, only the angles of which vary

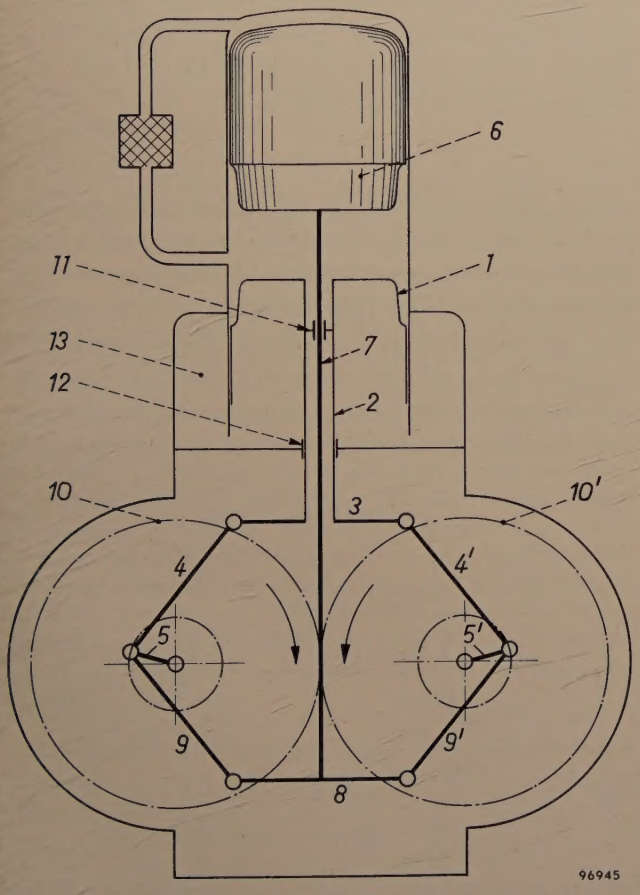

Fig. 9. Schematic diagram of rhombic drive mechanism. *1* = power piston. *6* = displacer piston. *5-5'* = cranks in two shafts rotating in opposite senses and coupled by gears *10-10'*. *4-4'* = con-rods pivoted from ends of yoke *3* fixed to the hollow power-piston rod *2*. *9-9'* = con-rods pivoted from ends of yoke *8* fixed to displacer-piston rod, which runs through the hollow power-piston rod. *11* and *12* = gas-tight stuffing-boxes. *13* = buffer space containing gas at high buffer pressure.

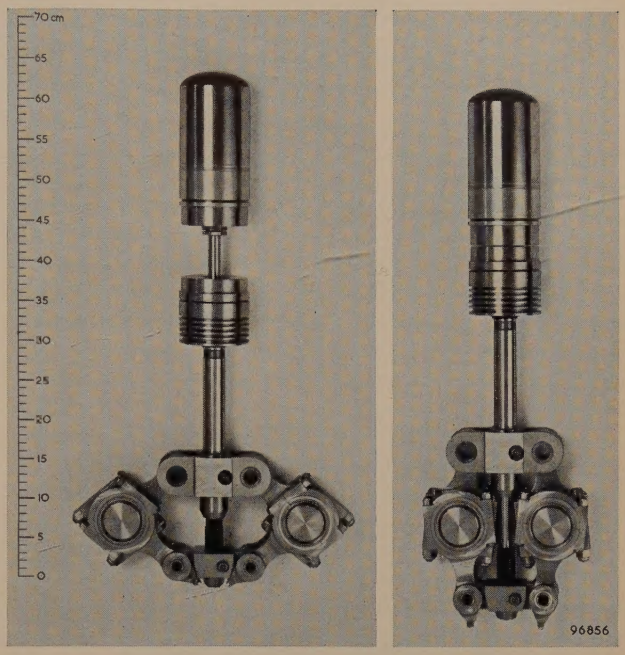

Fig. 10. Model of an actual rhombic drive mechanism, in two positions (cranks and gearwheels not present in this model).

when the system is in motion; it is for that reason that we have adopted the name "rhombic drive". Gearwheels *10-10'* ensure exact symmetry of the system at all times. The two crankshafts being geared together, the entire shaft output can be taken off either.

Fig. 10 shows a practical form of such a crank mechanism. The motion is illustrated by photographing the mechanism in two different positions (the cranks and the gearwheels are absent in this model).

The symmetry of the system and the coaxial arrangement of power-piston and displacer-piston rods make it an easy matter to avoid putting the crankcase under high pressure. The stuffing-box *11* for the displacer-piston rod is inside the hollow power-piston rod. One more seal, namely the stuffing-box round the power-piston rod (*12* in fig. 9), is all that is necessary to form a comparatively small cylindrical chamber *13* under the piston, separate from the crankcase; this "buffer space" can be filled with gas at the desired buffer pressure. The success of this arrangement depends essentially on the fact that the power-piston rod stuffing-box is subject to no lateral thrust, as *the horizontal components of the forces exerted by each pair of con-rods are exactly balanced at each yoke.* (That they do so, and that frictional losses are low in consequence, has the further advantage of enhancing the mechanical efficiency of the system.) The minimum permissible volume of the buffer space is determined

only by the range within which it is desired to limit the pressure variations inside the chamber. In a multi-cylinder engine the buffer chambers can be interconnected; this allows the volume of the individual spaces to be made even smaller.

In principle a space of this kind can be walled off under the piston in engines embodying the crank systems shown in figs. 7 and 8, but it is then necessary to have the rods running in a crosshead guide in order to prevent their gas-tight stuffing-boxes being acted upon by the horizontal components of the connecting-rod forces. This leads to considerable structural complications.

The power piston and displacer movements resulting from the new drive are displayed graphically in *fig. 11*, in the same way as in figs. 3 and 5. It will be seen that if the direction of rotation is as indicated in fig. 9, the volume variation of the hot space

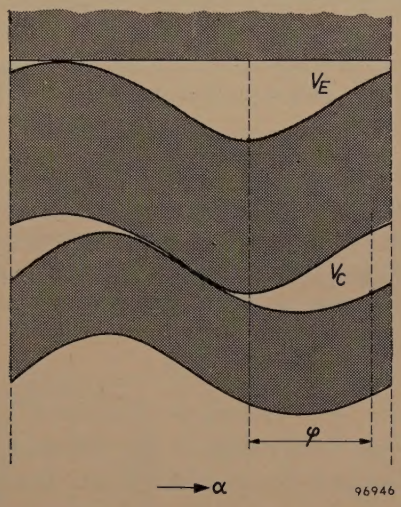

Fig. 11. Curves similar to those in figs. 3 and 5, showing the displacements undergone by the power and displacer pistons in a rhombic drive system such as that of fig. 9.

will have a phase lead with respect to that of the cold space, as is required. The power and displacer pistons do not by any means move in simple harmonic motion, but it is found that a very good version of the Stirling cycle is obtainable. This might seem surprising, for on the face of it the use of the rhombic drive may appear to have restricted the freedom of choice with regard to parameters w and φ (the amplitude ratio and relative phase of the variations in volumes V_E and V_C — see above), which play a large part in the design of a hot-gas engine. However, more exact analysis of the new drive shows that it is in fact possible, by altering the offset of the crankshafts, the proportions of cranks and con-rods and the ratio of power and displacer piston diameters, to vary these parameters over quite a wide range.

The balancing of the drive mechanism

The rhombic drive has the important property of allowing the designer of an engine even with only *one* cylinder to obtain complete dynamic balancing of the forces due to the inertia of moving parts, and of the moments of these forces — "complete" in the sense that the fundamentals *and* all the higher harmonics are balanced. We shall demonstrate this for the simple case where the con-rods are of equal length (as in fig. 9).

The configuration is given in *fig. 12*. On grounds of symmetry it is clear that the sum of all inertial forces acting horizontally is zero at any given instant. The same applies to all inertial-force moments about an axis perpendicular to the plane of the drawing. Hence all we need consider are the inertial forces acting in the vertical direction. We begin by resolving the circular motion of each crankpin T-T' into a vertical and a horizontal component. The vertical movements that the power and displacer pistons make as a result of the *horizontal* movement of the crankpins are equal and opposite because the con-rods are of equal length (symmetrical deformation of the "rhombus"). Hence, if the masses of the two pistons (including the rods etc. attached thereto) are made equal:

$$m_z = m_v, \quad \ldots\ldots \quad (10)$$

the sum of the vertical inertial forces corresponding to horizontal crankpin movement is always zero. There remain the vertical movements of power and displacer pistons as a result of the *vertical* component of the crankpin movement. These movements are exactly equal and, moreover, identical with the vertical movement of the crankpins. One can therefore imagine the moving mass of the two pistons,

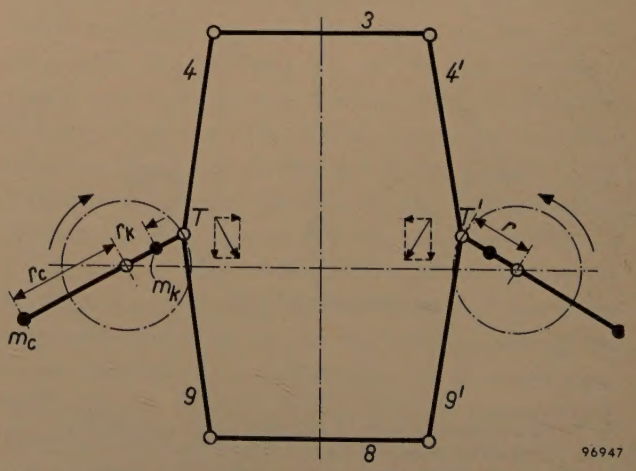

Fig. 12. Configuration of rhombic drive in which yokes *3* and *8* are of equal length, and all four con-rods *4-4'* and *9-9'* are equal. For discussing the inertial forces, the circular motion of crankpins T-T' can be resolved into vertical and horizontal components.

$m_z + m_v$, as localized in the crankpins, $\frac{1}{2}(m_z + m_v)$ in each. By means of two counterweights m_c mounted opposite each crankpin at a suitable radius r_c, vertical inertial forces can be created which exactly balance those of $(m_z + m_v)$ — and this is true even if the rotation of the crankshafts is not exactly uniform.

In fact, the mass and offset of each counterweight are chosen such that the latter also serves to balance the crank and other eccentrically positioned moving parts. If m_k is the effective mass of all these parts, and r_k the distance of their centre of gravity from the crankshaft axis, we have the following condition for balancing:

$$r_c m_c = \tfrac{1}{2} r(m_z + m_v) + r_k m_k . \quad . \quad . \quad (11)$$

From the foregoing it will be clear that the reason why it is possible in this way to balance the inertial forces in a displacer type of engine is that, even for single-cylinder machines, there are *two* reciprocating masses whose movements differ in phase [8]). In order to satisfy the condition $m_z = m_v$ it will generally be necessary to make the masses of the two pistons themselves different. This should not involve any difficulty, for the two bodies have different shapes and different functions and are not interchangeable.

The configuration of fig. 12 is a special case of a much more general form of the new drive. We obtain the more general form by abandoning the restriction that the pairs of connecting rods are equal in length, and by allowing each displacer-piston con-rod to hinge not on the crankpin but about any arbitrary fixed point on the power-piston con-rod (see *fig. 13*). In this general form, which design considerations may render more attractive than the special one of figs. 9 and 11, the power and displacer piston rods continue to move coaxially without the presence of any lateral thrust. This means that the expedient of the buffer chamber with gas under pressure can again be applied without complications. Moreover — and perhaps surprisingly — it can be shown that the inertial forces of the moving parts of the general form of this drive mechanism can be completely balanced as before, provided certain straightforward conditions are fulfilled. We shall state these conditions here without proof. For balancing to be possible the parameters of the mechanism as indicated in fig. 13 must satisfy the equations:

$$\left.\begin{aligned} &\Delta e = 0 , \\ &c = \sqrt{1 - 2\frac{a}{l}\cos\beta + \left(\frac{a}{l}\right)^2} , \\ &m_1 - m_4 + \frac{a}{l}(m_3 + 2m_4)\cos\beta = 0 . \end{aligned}\right\} \quad . \quad . \quad . \quad (12)$$

The net inertial force can then be completely balanced by fitting counterweights whose positions and masses are given by

$$\gamma = \pi - \tan^{-1} \frac{\frac{a}{l}(m_3 + 2m_4)\sin\beta}{m_1 + m_2 + m_3 + m_4 + \frac{r_k}{r} m_5}$$

and

$$m_6 = \frac{r}{r_c} \sqrt{\left(m_1 + m_2 + m_3 + m_4 + \frac{r_k}{r} m_5\right)^2 + \left\{\frac{a}{l}\left(m_3 + 2m_4\right)\sin\beta\right\}^2} \quad . \quad . \quad . \quad (13)$$

respectively. It will be seen that when a is zero, as it is in the special case first discussed, these conditions transform into the simple ones given earlier.

The particular version of the hot-gas engine with which we shall concern ourselves in this article has the simple form of crank mechanism shown in fig. 9.

In addition to inertia forces, an *alternating moment* acts on the foundation of every piston engine when under load as a consequence of the periodic variation of the torque produced on the shaft. With the rhombic drive mechanism (either the special or the general form) a relatively simple expedient makes it possible to balance out a large part of this alternating moment. It is only necessary to fit two flywheels instead of the usual one, one on each of the two oppositely-rotating crankshafts.

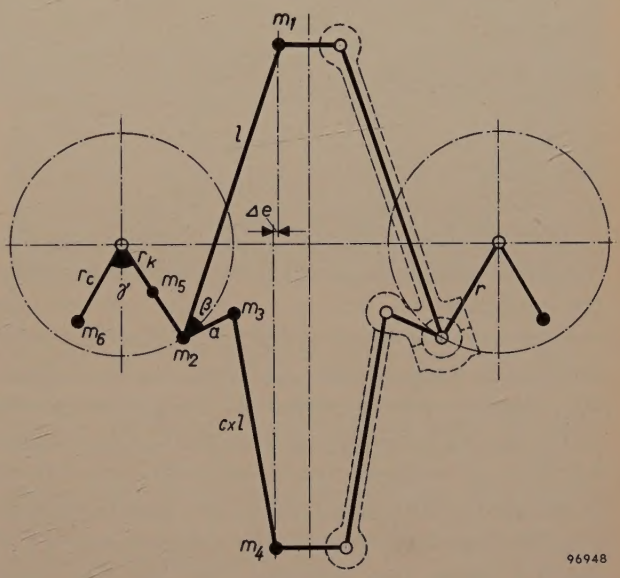

Fig. 13. General form of the new drive. $m_1 \ldots m_6$ are the masses of the moving parts, imagined localized at various points for the purpose of deriving the conditions for the balancing of inertial forces and moments.

Further constructional details of the engine

The general appearance and layout of the experimental engine may be seen in *fig. 14*. *Fig. 15* is a cross-sectional sketch, burner and pre-heater not being shown; for the sake of clarity some of the parts have not been drawn exactly to scale. The notation of the drive mechanism is the same as in preceding diagrams; the counterweights are also shown (*14*).

[8]) It is clear that the rhombic drive could also be used for attaining complete dynamic balancing in internal-combustion engines, but it would probably be a proposition only in engines with at least two cylinders, i.e. in which at least two pistons are in reciprocating motion.

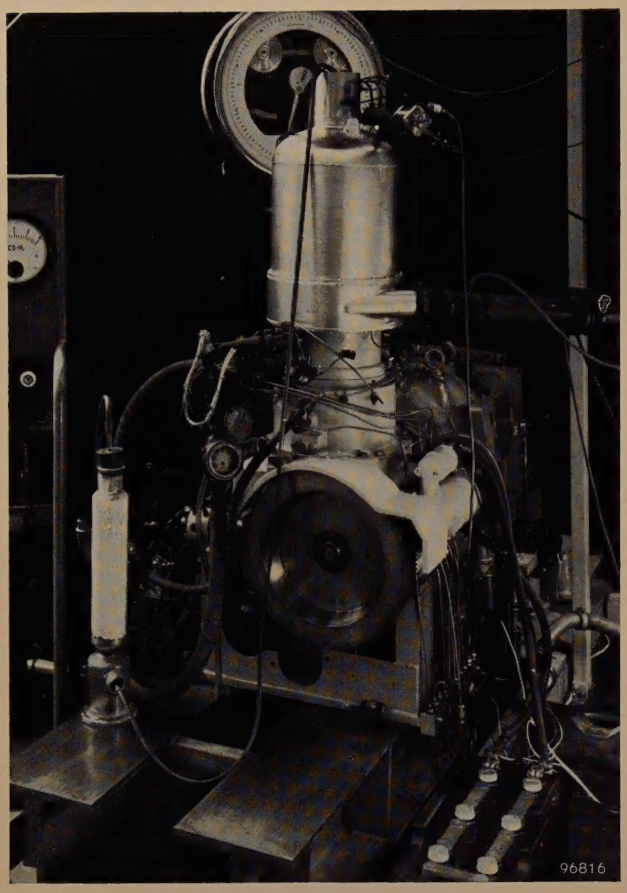

Fig. 14. Experimental model of the Philips hot-gas engine with rhombic drive, in position on the test bench.

As in previous designs described in this Review[3]), the cooler, regenerator and heater all have an annular configuration, and are mounted around the expansion-compression cylinder. This arrangement makes for compactness, and low gas-flow losses. The displacer piston consists of the piston base *6a* and a thermally insulating dome *6b*. The piston base fits like an ordinary piston into the cylinder *16* at the level of the cooler. There is a small clearance between the dome *6b* and the cylinder wall *15* of the hot space, just sufficient that the two never come into contact. Underneath the power piston the buffer chamber *13* can be seen.

The design of the *regenerating casing* has undergone a good deal of modification. In the first version of the experimental engine the regenerator casing was a comparatively flat annular body (*fig. 16*); the cylinder wall *15* formed the inner wall, the outer wall *a* being joined to the cylinder via perforated flange *b*. Considerable stresses were set up in the walls of the casing owing to expansion of the upper side as its temperature rises to the high value T_E, the lower side remaining at the low temperature T_C. Efforts to step up the output of the hot-gas engine were soon brought to a halt by the thermal stresses arising in this way, these becoming excessive especially as the working pressure of the engine was raised. The difficulty has been avoided by dividing up the annular regenerator space into a number of

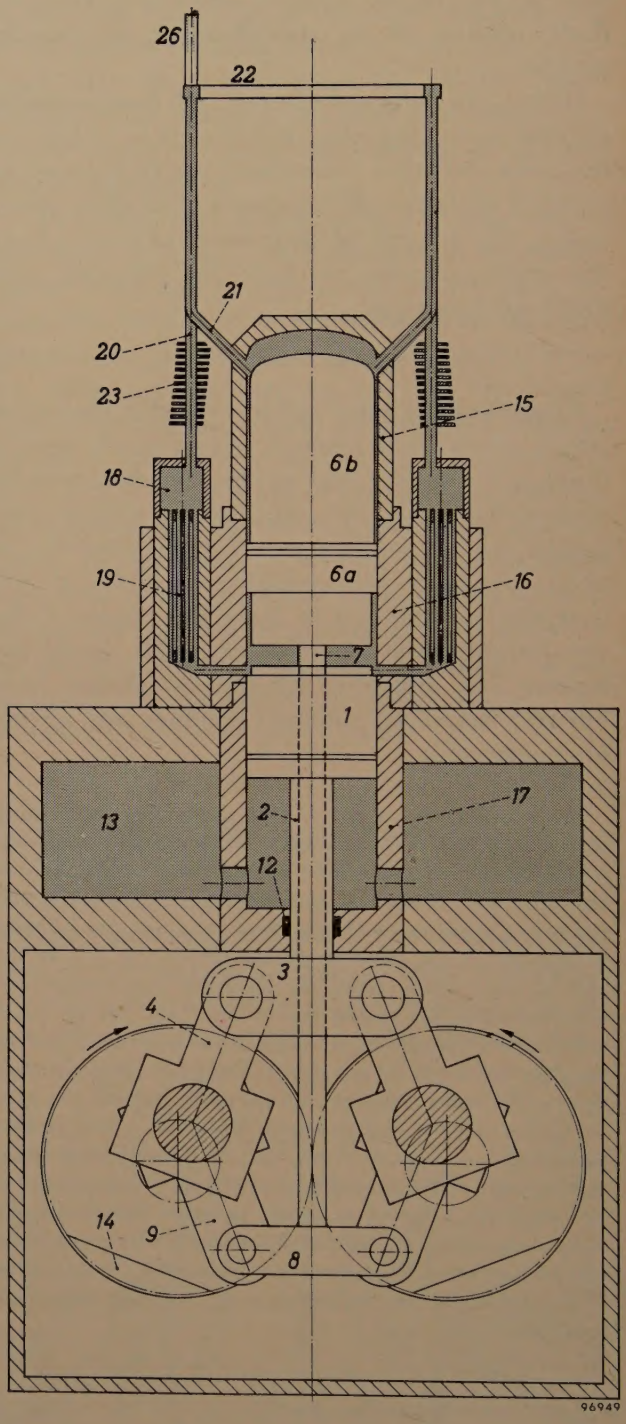

Fig. 15. Cross-section of the engine shown in fig. 14, much simplified and, for the sake of clarity, not entirely drawn to scale. The burner and air pre-heater are absent; they are shown separately in fig. 18. Spaces filled with hydrogen are shaded. *1* = power piston. *6a* and *6b* = displacer piston and insulating dome. *12* = power-piston stuffing-box. *13* = buffer chamber. *14* = counterweights. *15*, *16*, *17* = cylinder in which power piston and displacer piston move. *18* = regenerator compartment. *19* = cooler compartment, *20*, *21*, *22* = heater tubes. *23* = fins. *26* = tube for temperature probe. Other symbols as in fig. 9.

small chambers ("cups") not contiguous with the cylinder wall; see *fig. 17*. Thermal stresses in the regenerator wall then ceased to be a problem. Furthermore, it was now possible to ensure that the lines of principle stress ran substantially straight from the head of the cylinder *15* via the cylinder

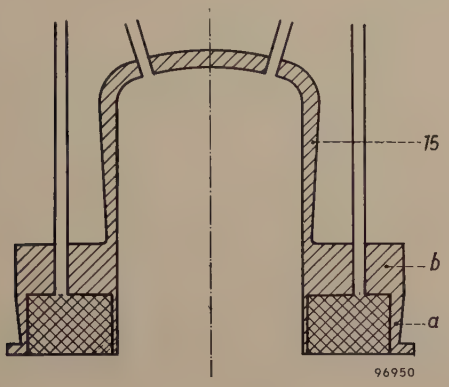

Fig. 16. Earlier design of regenerator compartment, with cylindrical outer wall *a* attached to cylinder wall *15* by means of perforated flange *b*.

wall *16*, *17* to the base of the latter cylinder (see fig. 15). In earlier designs embodying the flange mentioned above, these lines tended to curve outwards, which meant that the flange had to withstand a strong bending moment. The new design allows the whole assembly to be kept comparatively light despite the high maximum pressure of the gas.

The design of the cooler has been adapted to that of the regenerator. The cooler housing *19* contains a number of tubes bunched together in groups (cooler "units"), the end of each unit protruding into one of the regenerator cups. The tubes of each cooler unit are mounted with a *sliding fit* in the cooler housing; in this way the regenerator cups are left free to undergo small longitudinal displacements consequent on the expansion of the heater tubes.

The heater consists of two sets of pipes, *20* and *21*, in close-packed configuration but with small clearances. The hot gases from the burner are blown between these tubes in a direction perpendicular to their length. The tubes of set *20* terminate inside the regenerator cups (see figs. 15 and 17); gas from the regenerator streams upward through these tubes into the annulus *22*, whence it is carried downwards by the tubes of set *21*, which are brazed into the hot end *15* of the cylinder. To improve the heat transfer between the combustion gases and the working gas, a series of fins *23* are brazed to the pipes of set *20*.

The heater is surrounded by the air *pre-heater* (*27* in *fig. 18a*), which functions in the following way. The air necessary for combustion enters the

Fig. 17. New design of regenerator compartment and heater. The regenerator (below) is now split up into a series of cups surrounding but not touching the displacer cylinder. The new design solved the thermal-stress problem. It will be seen that three tubes issue from each regenerator cup, their extensions forming the vertical heater tubes that carry the upward-streaming gas. Alternating with these, and connected to them via the annulus at the top, are downward-flow tubes that lead to the head of the cylinder. The lower part of this tube system is fitted with fins in order to improve the heat transfer from the combustion gases to the tubes.

lower end of channels A_1 situated around the outer perimeter of the air pre-heater (fig. 18*b*) and then flows via the spaces A between the spirally curved partitions into the channels A_2 around the inner perimeter and thence, upwards, to the burner. The exhaust gases, which leave the burner with a temperature somewhat higher than that of the heater, enter channels B_1 around the inner perimeter and flow via B, a second set of spiral spaces lying between the A spaces, in a direction opposite to that of the incoming air, to the channels B_2 around the outer perimeter of the air pre-heater. It has proved pos-

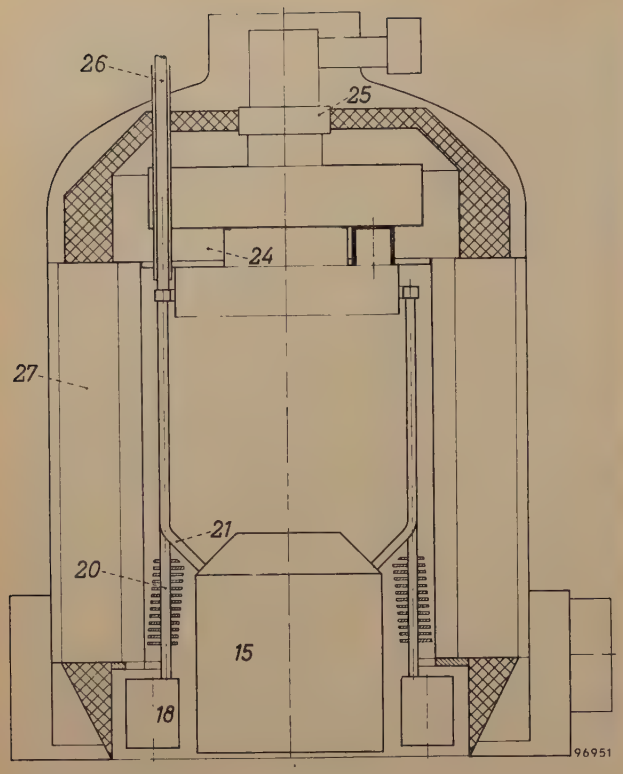

a

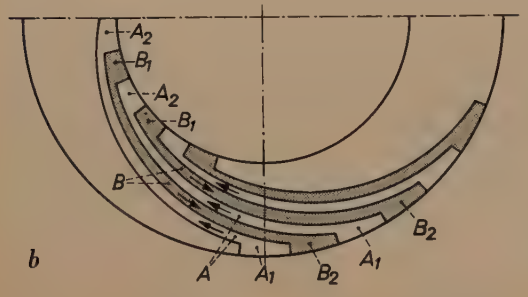

b

c

Fig. 18. *a*) Cylinder head of engine, surmounted by burner *24*, atomizer *25* and surrounded by air pre-heater *27*. Other symbols as in fig. 15.
b) Cross-section through air pre-heater, showing the narrow *A* and *B* spaces which lie between the spirally curved partitions and through which pass, in opposite directions, fresh air for and spent gases from the burner. The air enters via the lower end of the channels A_1 and leaves via the upper end of A_2, both sets of channels running parallel to the cylinder axis. Similarly the burnt gases enter via the lower end of channels B_1 and leave via the upper end of channels B_2, likewise parallel to the cylinder axis.
c) View of air pre-heater, which fits over the heater shown in fig. 17.

sible on this principle to build a very compact pre-heater (fig. 18*c*) with low resistance to air flow. Moreover, the pre-heater "insulates itself"; all the channels around its outer perimeter (A_1 and B_2) are near the ambient temperature.

The *burner* (*24* in fig. 18*a*) is of the "swirl-chamber" type, which can be used in conjunction with a large number of fuels possessing widely differing properties, such as coal gas, propane, butane, kerosene, diesel oil and light fuel oil. If liquid fuels are to be used, the burner is fitted with an atomizer *25*, which sends a fine spray of the liquid into the upper part of the burner.

Regulation of engine output

It will be seen from formula (7) that the power output of the hot-gas engine can be controlled very conveniently by altering $\bar{p}$, the mean pressure of the working gas; changing $\bar{p}$ has no effect on the thermal efficiency (eq. 8) of the engine, provided the cooler and heater temperatures remain unaltered. To fulfil this proviso a separate automatic regulator is required. (The overall efficiency is in fact somewhat affected by a pressure change because, in addition to the effect mentioned under [7]), the absolute magnitude of some — less important — losses remains practically constant; the effect can be deduced from fig. 21 below.)

Accordingly, the control system of the hot-gas engine falls into two parts:

1) A system for admitting gas to and withdrawing it from the engine in order to adjust the pressure to give the output required (i.e. the braking torque), while maintaining the (pre-set) speed of the engine constant.
2) A system for controlling the fuel supply to the burner in such a way that the temperature of the heater remains steady when the power output (and hence the rate at which heat has to be

supplied) is changed. For this purpose, control action is exercised by a thermostat, the temperature-sensitive element of which is inserted, for example, in the stream of gas through one of the heater pipes (through tube *26* in fig. 15; in the heater of fig. 17 two such tubes are incorporated).

The control system for regulating the pressure will be discussed here.

Regulation of the pressure in the engine described here is effected by a set of hydraulically operated valves. A diagram of the system is given in *fig. 19*. The governor *1*, which is driven by the engine shaft, ensures that, at the nominal speed to which the governor causes the oil pressure in pipes *2* and *3* to drop, with the result that valve *9* of the regulator *10* opens up, whereby allowing gas from the cylinder to flow via non-return valve *11* to the inlet of a small auxiliary compressor *12*, whence it passes into the tank *6*. The release of gas from the engine continues until the nominal speed is attained (whereupon valve *9* closes).

As stated above, the buffer space *13* under the piston (see also fig. 15) is filled with gas at a buffer pressure; this pressure must also undergo adjustment in accordance with changes in the load. The engine under discussion has been designed for a buffer pres-

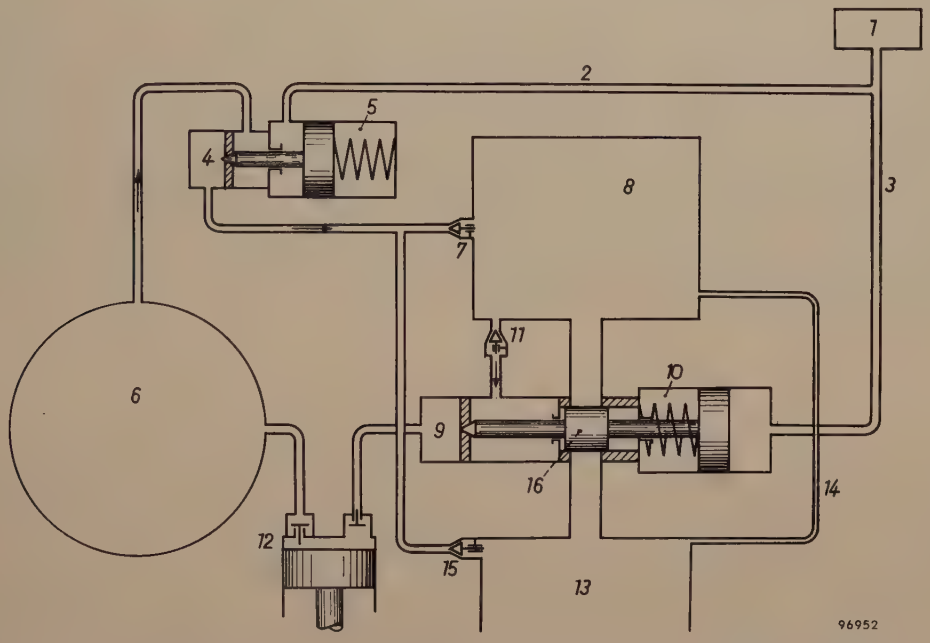

Fig. 19. Hydraulic mechanism for regulating the output of the hot-gas engine. By altering the oil pressure in pipes *2* and *3*, governor *1* controls the operation of valves *4* and *9*. If the engine speed falls below the pre-set value, gas from the tank *6* flows via valves *4* and *7* into the cylinder *8*; if the speed setting is exceeded, gas passes from *8* via valves *11* and *9* and compressor *12* back to *6*. The function of the slide throttle *16*, which connects the cylinder with the buffer space *13*, is to ensure a rapid response when the load is reduced suddenly.

engine has been adjusted to run, a certain oil pressure is maintained in pipes *2* and *3*. If the engine slows down slightly in consequence of an increase in the braking torque, the governor raises the oil pressure in those pipes, with the result that valve *4* in the feed device *5* opens up, and gas from tank *6* passes via feed valve *7* into the space *8* which represents the cylinder of the hot-gas engine. Pressure inside the engine having risen accordingly, its power output increases. The injection of additional gas continues until the engine speed has reverted to the original setting (whereupon valve *4* closes). If the speed increases slightly in consequence of a decrease in the braking torque, the sure equal to $\bar{p}$, the mean pressure in the cylinder. In principle this buffer pressure is obtained automatically, by means of a capillary tube connecting the buffer space with the cylinder. We shall return presently to other provisions made for this purpose.

The auxiliary compressor gives a gas-tank pressure rather higher than the minimum pressure in the cylinder under conditions of full load. For increasing the engine output, therefore, it is possible to inject additional gas via valve *7* until the full power is developed. This adjustment takes place very rapidly. When it is a question of reducing the output, for example from full power, the auxiliary compressor initially performs no function

because gas from the cylinder returns to the tank via valves *11* and *9* under the excess pressure in the cylinder; this continues until the maximum pressure in the cylinder has dropped to the tank-pressure value. This too happens very quickly. If, however, the cylinder pressure is to be lowered still further, then the auxiliary compressor must function, and thereafter it is this that determines the speed of response. If a *sudden* decrease in the load (e.g. sudden removal of the whole braking torque) is not to result in racing of the engine, the compressor required would have to be very large. This difficulty has been overcome by incorporating an additional regulating mechanism. Besides opening and closing valve *9*, regulator *10* actuates a slide throttle *16* which offers the gas a direct path between cylinder and buffer chamber; the escape of gas will be large or small in accordance with the magnitude of the change in the load. It is clear that this gas escape path is equivalent to a leak past the power piston: it causes a certain decrease of the useful power delivered by the engine (which is now indeed associated with a decrease in efficiency; whence the term "loss-regulation", coined for this control). Because the action of the slide throttle has an almost instantaneous effect, a very small auxiliary compressor is adequate [9]).

In consequence of the direct connection between cylinder and buffer space when the power of the engine is being reduced, the buffer pressure likewise adjusts itself almost immediately to the correct value. This quick readjustment is highly desirable, since it limits unnecessary asymmetrical thrust on the drive mechanism. A similar purpose is served by valve *15*. It prevents the buffer pressure lagging too much when output is suddenly *raised* to a much higher value: if the value from which it is raised is so low that the mean pressure in the cylinder is less than the tank pressure, gas from the tank will pass directly into the buffer chamber via valves *4* and *15*.

Engine data and test results

We now give the more important data relating to a single-cylinder hot-gas engine designed and built in Philips Research Laboratories, Eindhoven, along the lines described above.

Cylinder bore	88 mm
Power-piston stroke	60 mm
Nominal engine speed	1500 r.p.m.
Mean piston velocity at 1500 r.p.m.	3 m/sec
Highest permissible value of p_{max}	140 kg/cm² (≈140 atm)
Mean pressure $\bar{p}$ corresponding to the above value of p_{max}	105 kg/cm² (≈105 atm)
Compression ratio p_{max}/p_{min}	2.0
Nominal cooling-water temperature	15 °C (≈60 °F)
Nominal heater temperature	700 °C (≈1290 °F)
Working fluid	Hydrogen
Fuel	Light fuel oil

We have already alluded to the advantages of hydrogen as the working fluid; the flow losses are relatively small and good heat transfer is attainable, the efficiency being thereby greatly enhanced. In addition, the speed of response of the engine to changes in the load or controls, which is ultimately determined by the effective cross-sectional areas of ducts and valves in the regulating system, is improved by using a low-density gas.

The results of measurements of the brake horsepower and specific fuel consumption of the engine will now be dealt with. The efficiencies derived from these figures relate to the engine without auxiliary devices [10]) and are based on a fuel of calorific value (low heat value) 10000 kcal/kg (≈18000 B.T.U./lb). The measurements were made at four different pressure levels corresponding to p_{max} values of 50, 80, 110 and 140 kg/cm², and at six different engine speeds for each of these pressure levels, namely at 250, 500, 1000, 1500, 2000 and 2500 r.p.m. *Fig. 20* is a general view of the equipment used for the measurements. In *fig. 21* the measured power and overall efficiency are plotted as functions of the engine speed in r.p.m. It will be noted that a power of up to 40 H.P. can be developed and that the overall efficiency has a maximum value of 38%. In addition, the measured torque is plotted

[9]) In a multi-cylinder engine we arrange for the leakage to take place in a rather different manner: the slide throttle opens a gas path from one cylinder to the next. This is equally effective because neighbouring cylinders must in any case differ in phase. Thus the one throttle provides instantaneous "loss regulation" for two cylinders.

[10]) Apart from the usual pumps and fans for forced oil feed and cooling, the auxiliaries comprise the regulating compressor already mentioned and a blower for the burner. Of all these the latter absorbs the most power, viz. 1 to 2% of the engine output.

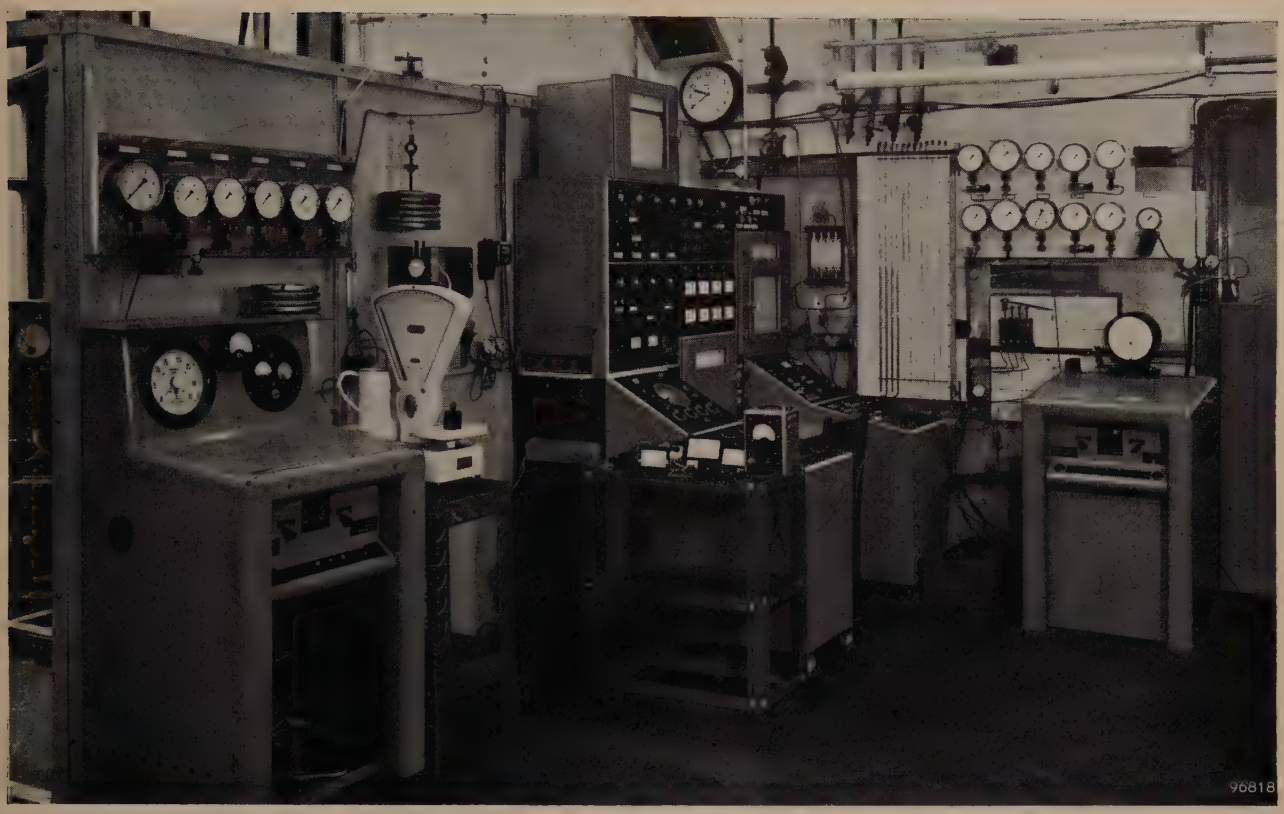

Fig. 20. Equipment used for measuring the torque, shaft power and efficiency of the hot-gas engine under widely differing conditions.

in *fig. 22* for the highest working pressure, for which $p_{max} = 140$ kg/cm². The unusual flexibility of the engine is apparent from the small variation in the torque (11.5 to 15 kg.m or 80 to 110 lb.ft) at greatly different speeds. Equally remarkable is the fact that the overall efficiency varies only slightly over a considerable range of speeds and pressures.

It is the usual practice to display the results of

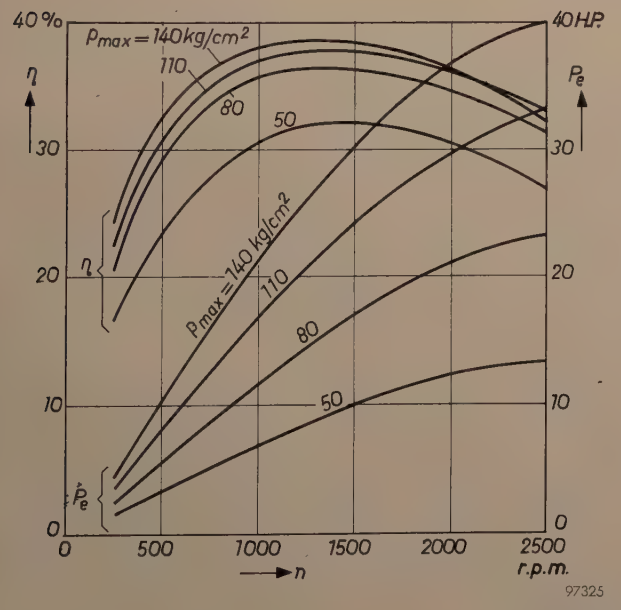

Fig. 21. Measured shaft power P_e and efficiency η of the experimental version of the new Philips hot-gas engine with rhombic drive, plotted as functions of the engine speed for various values of p_{max}.

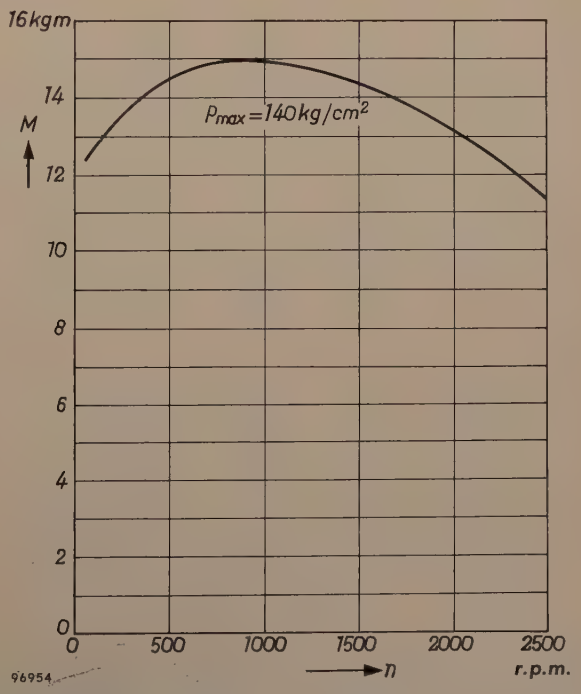

Fig. 22. Measured torque M as a function of the engine speed, for the highest admissible pressure level.

engine tests in a graph such as that of *fig. 23*. Here the coordinates are the engine speed and p_e, the "mean effective pressure" (m.e.p.). This latter is not the mean gas pressure actually occurring in the engine but merely a formal ratio, being defined as the work done by the shaft per revolution divided by the volume swept by the piston; hence the product of p_e and n, the speed in r.p.m., is the specific power output. For a given engine, therefore, every point in the p_e,n diagram corresponds to a definite value of the power developed P_e, and the curves of constant P_e are hyperbolae, in view of the fact that

$$p_e . n \propto P_e . \quad . \quad . \quad . \quad . \quad (14)$$

In such a diagram contours of constant specific fuel consumption (grams of fuel per horsepower-hour, output measured at the shaft) are now drawn.

Fig. 23*a* shows these curves for the experimental engine. The upper boundary to this family of curves, indicated by a broken line, is due to the ceiling on the gas pressure in the cylinder; in the present case the highest permissible pressure is 140 kg/cm², and consequently P_e for a given engine speed cannot exceed the value corresponding to that pressure.

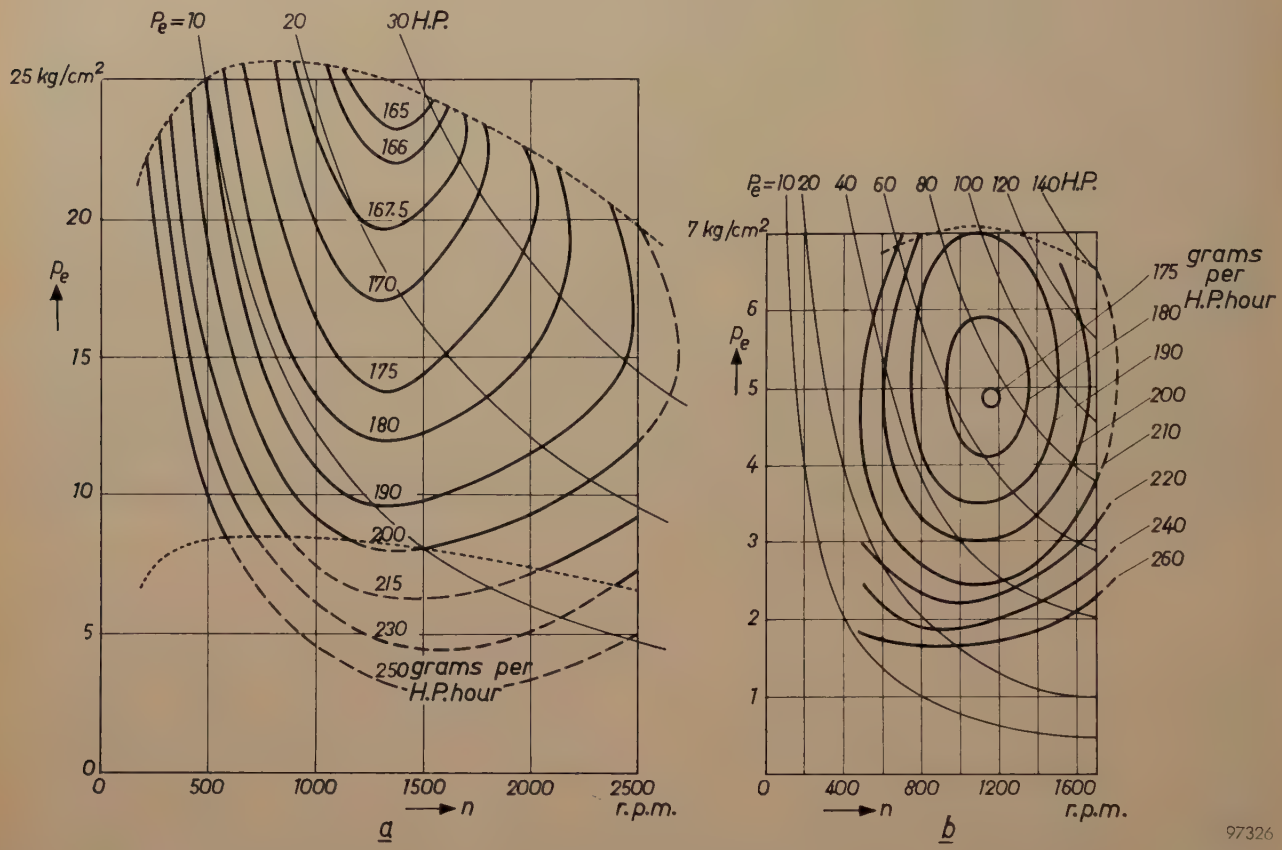

Fig. 23. *a*) Curves of constant specific fuel consumption (in grams of fuel per H.P. hour; for lb per H.P. hour divide by 453) are drawn here in the p_e,n diagram for the hot-gas engine. p_e is the mean effective pressure (m.e.p.) defined as the useful work done by the shaft per revolution divided by the volume swept out by the piston. Accordingly, $p_e . n \propto P_e$, which means that, for a given engine, every point in the diagram corresponds to a definite value of the power P_e and that the curves of constant P_e (lightly drawn in the diagram) are hyperbolae. The broken line representing the upper limit to the measurements corresponds to the pressure ceiling of $p_{max} = 140$ kg/cm² (this curve is derived from the P_e curve for this pressure, given in fig. 21, simply by dividing each ordinate by the corresponding abscissa). The broken line representing the lower limit corresponds to the lowest pressure level at which measurements were made, corresponding to $p_{max} = 50$ kg/cm².
b) p_e,n diagram for a diesel engine (after J. M. Kuijper, Dieselmotoren, Stam, Haarlem 1954, page 81, fig. 52).

(The lower boundary to the curves is not an actual restriction on the engine; it corresponds to the lowest pressure at which measurements were carried out, namely $p_{max} = 50$ kg/cm². The broken-line portions of the curves of constant specific fuel consumption, which lie beneath the lower limit, have been extrapolated.)

The striking thing about the diagram is that the curves do not form complete loops, as they do in the corresponding diagram for a diesel engine, for

example — see fig. 23*b*. This means that the hot-gas engine achieves its highest efficiency at an m.e.p. which lies close to the highest permissible value. This highest permissible value is here not determined by a "smoke-limit" as in a diesel engine, but simply by the strength of the engine casing. In making such a comparison, however, it should be emphasized that *m.e.p. values alone are quite useless* (and so is the specific power output) *as a yardstick for comparing the hot-gas engine with internal-combustion types* from the standpoint of *bulk*. The fundamental differences are too great. A better yardstick is the specific weight, that is, the weight per horsepower.

All the above values were measured with the nominal heater and cooler temperatures given earlier. The effect of changes in these temperatures on output and efficiency may be seen in *figs. 24a* and *b*. The curves given are appropriate to an engine speed of 1500 r.p.m. and a p_{max} of 140 kg/cm².

Finally, *figs. 25a* and *b* are graphs showing the heat balance of the engine plotted as a function of p_e (at $n = 1500$ r.p.m.) and as a function of n (at $p_{max} = 140$ kg/cm²) respectively. The narrowness of the band representing flue losses shows the effectiveness of the air pre-heater: over a large range of n and p_e values the burner has an efficiency of

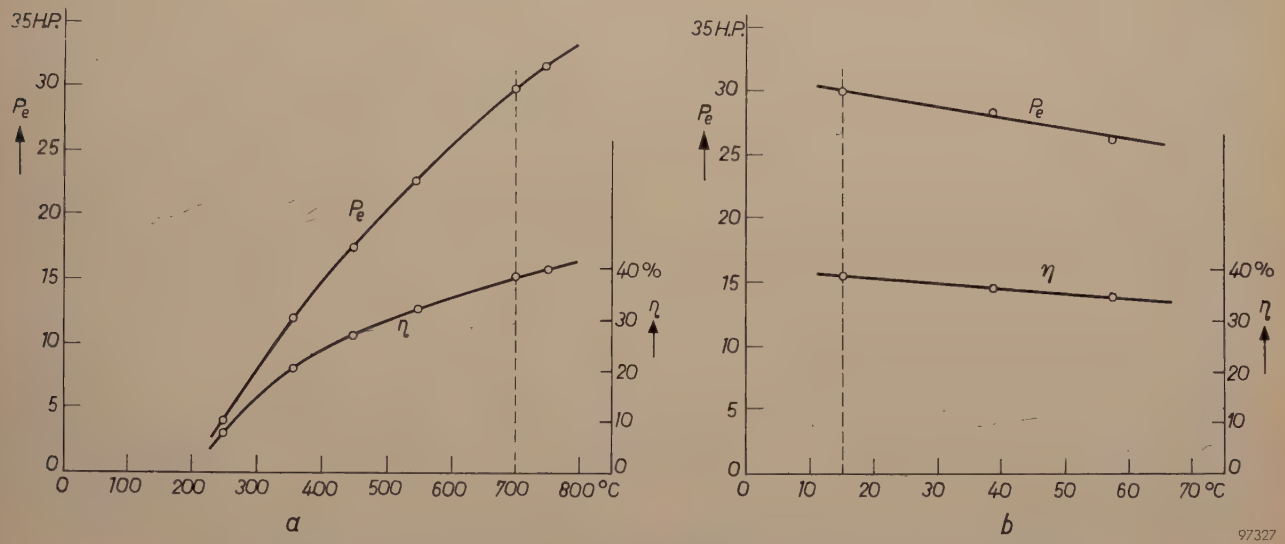

Fig. 24. Shaft power and efficiency of the experimental hot-gas engine as functions of (*a*) the heater temperature and (*b*) the cooler temperature. The curves are those appropriate to an engine speed of 1500 r.p.m. and a p_{max} of 140 kg/cm².

Although few special measures were taken to keep the weight of the present experimental engine low, the specific weight is in fact only 5 kg per H.P. (11 lb per H.P.).

The following are the extreme values found for various quantities.

Maximum shaft output P_e *)	40 H.P.
Maximum mean effective pressure p_e **) . . .	26 kg/cm²(~ 26 atm)
Maximum torque **) .	15 kg.m (~110 lb.ft)
Maximum specific power output *) (H.P. per litre swept volume of piston)	120 H.P./litre
Minimum specific fuel consumption ***) . .	165 grams/H.P.hour (0.36 lb/H.P.hour)

*) Occurs at $n = 2500$ r.p.m. and $p_{max} = 140$ kg/cm².
**) Occurs at $n =$ approx. 800 r.p.m. and $p_{max} = 140$ kg/cm².
***) Occurs at $n =$ approx. 1350 r.p.m. and $p_{max} = 140$ kg/cm².

over 90%. Chief amongst what are shown as "other losses" are those due to mechanical friction. The item may also include losses due to incomplete fuel combustion ("non-detectable" flue losses). One cannot expect these "other losses" to be specified with any great accuracy, but from the good reproducibility of the results, we may reasonably conclude that the mechanical efficiency of this rhombic-drive engine is high.

Concluding remarks

To end with, we may recall here the essential features of the hot-gas engine in general (cf. [2])):

a) Liquid and gaseous fuels of greatly differing properties can be used, little modification of the engine being necessary.

b) Lubricating-oil consumption is low and there is little wear, owing to the absence of corrosive substances and to the relatively low piston velocity.

c) Noise level is very low.

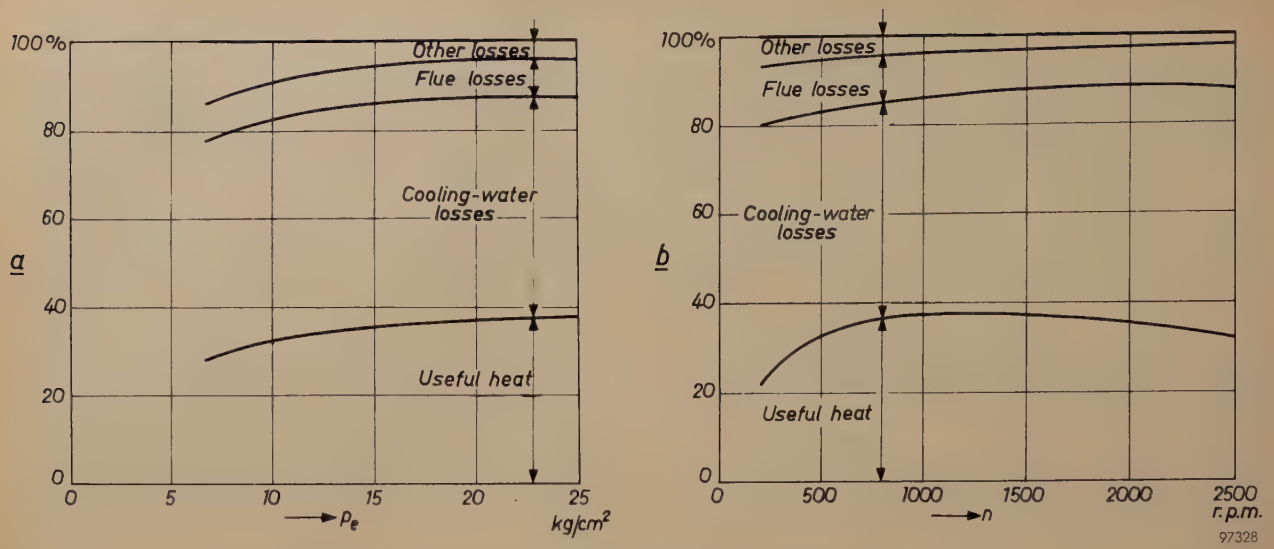

Fig. 25. Heat balance for the experimental hot-gas engine (a) as a function of p_e at n = 1500 r.p.m., and (b) as a function of n at p_{max} = 140 kg/cm².

d) The torque varies only slightly over a large range of engine speeds.

e) The torque variation as a function of the crank angle is relatively small. In this respect a single-cylinder hot-gas engine is comparable with a four-cylinder internal-combustion engine.

In addition to these general features, the experimental engine described here converts heat into mechanical energy with a high efficiency, as the results of our measurements illustrate. Moreover it has been shown that good values of the weight per horsepower are attainable. These favourable qualities are mainly to be attributed to three features of the design: the use of a displacer piston with its attendent aerodynamic and thermodynamic advantages, the use of hydrogen as the working fluid, and the use of high working pressures. A further advantage of the newly developed engine is its freedom from vibration, in consequence of the complete dynamic balancing of the inertial forces of moving parts.

Summary. After a brief recapitulation of the hot-gas cycle as applied to an engine provided with a displacer piston, certain new design features of the Philips hot-gas engine are described. An account is given of a new kind of drive mechanism in which the required power and displacer piston movements are obtained by means of twin crank and con-rod mechanisms offset from the engine axis; the crankshafts are coupled by two gear-wheels, and rotate in opposite senses. Where such a system is used, the buffer pressure that is desirable under the power piston can be contained in a relatively small cylindrical buffer chamber — there is no need to pressurize the whole crankcase. The new drive mechanism also permits complete dynamic balancing of the inertial forces of moving parts, even in a single-cylinder engine. Other innovations concern the design of the regenerator compartment, the cooler and the heater: an entirely new approach has cleared up the problem of thermal stress in these components, whose weight can be kept quite low despite the high gas pressure. The pre-heater has also been redesigned, with the result that burner efficiencies of up to 90% are now reached. In addition, a fast-acting system has been developed for regulating the engine output, this being controlled by altering the mean working pressure of the gas in the cylinder.

These various features have been applied in the design and construction of an experimental single-cylinder engine of about 40 H.P., containing hydrogen (helium could also be used) as the working fluid and burning light fuel oil. The highest pressure permissible in the cylinder is 140 kg/cm². The nominal speed of the engine is 1500 r.p.m. Extensive tests on this engine, the results of which are given in the article, show that with the heater temperature at 700 °C it attains an overall efficiency of up to about 38% (engine alone, without auxiliaries). The maximum value of the specific power was found to be 120 H.P. per litre swept volume and the best specific fuel consumption 165 grams (0.36 lb) per H.P. hour. The specific weight of the engine is 5 kg (11 lb) per H.P.

SIGNAL-TO-NOISE RATIO AND DEAD TIME OF A SCINTILLATION COUNTER

by J. A. W. van der DOES de BYE.

621.387.464

In a scintillation counter a high ratio between the peak amplitudes of scintillation and noise pulses is obviously desirable. For some applications, moreover, the highest possible counting rate is required. This article discusses the design of the electronic equipment in the light of these considerations and describes how — since the two requirements conflict to a certain extent — a favourable compromise can be achieved in a given case.

In a scintillation counter used for detecting gamma quanta, each absorbed γ-quantum gives rise to an electrical pulse, the height of which may have any value between zero and a certain maximum. A fraction of these pulses will not be passed by the discriminator, the function of which is to transmit only pulses greater than a preset minimum amplitude and so to suppress the majority of the noise pulses. For a given type of scintillator, with given dimensions, this fraction can be smaller the relatively lower is the height of the noise pulses. The ratio between this height and the height of the scintillation pulses can be varied within certain limits by appropriately designing the electronic circuit.

Together with the fluorescence decay constant of the scintillating material, the electronic circuit also governs the minimum value that can reasonably be chosen for the *dead time* of the equipment, i.e. the time during which the counting system cannot react to a new pulse supplied to it. This dead time determines the maximum number of quanta or particles that can be counted per second. In this article we shall examine the influence of the electronic circuit on the two above-mentioned characteristics of a scintillation counter. We shall see that these characteristics cannot be varied entirely independently of each other. The theory shows, however, the means of obtaining, for a given dead time, the most favourable ratio between the amplitudes of scintillation and noise pulses — the *signal-to-noise ratio*. It also shows what sacrifice we must make with regard to the dead time in order to achieve a certain signal-to-noise ratio.

Our calculations will be based on the formulae which describe a scintillation pulse and a noise pulse as a function of time. For deriving the first of these formulae it will be convenient to begin with a brief recapitulation of the way in which the absorption of a γ-quantum in the scintillator gives rise, via the scintillation effect, to the occurrence of a pulse.

Scintillation pulses and noise at the amplifier input

Scintillation pulses

As explained in an earlier article [1]), a γ-quantum incident on the scintillating material gives up its energy E_0 wholly or partly to one or more electrons. These electrons in turn transfer the energy E_1 they have received to other electrons in small portions, giving rise to excitation in the scintillator. Some of the latter electrons in returning to the ground state, cause the emission of light quanta. The light quanta following upon the absorption of one γ-quantum together constitute a scintillation. In a good counter a large fraction of these scintillations can reach the photocathode of the photomultiplier tube. However, by no means all the quanta incident on the photocathode give rise to the emission of a photoelectron capable of entering the dynode system.

It is evident from the above that the average energy E_i which a γ-quantum must transfer to the scintillator in order to cause one useful electron to be emitted by the photocathode is substantially larger than the portions in which the primarily liberated electrons give up their energy. In the most commonly used scintillating material, NaI(Tl), the minimum value of E_i, which we term the *liberating energy*, is about 450 eV, which in this material does not depend on E_1.

Let g be the current gain of the multiplier tube, ε the charge of the electron and t the time, then the form of the current pulse delivered by the tube after the absorption of a γ-quantum, is given by [2]):

[1]) J. A. W. van der Does de Bye, Philips tech. Rev. **20**, 209-219, 1958/59 (No. 8). We shall refer to this article henceforth as I.

[2]) The current and voltage measured at the anode impedance of the multiplier tube will be denoted by i' and V'; the voltage measured at the amplifier output by V.

$$i'(t) = \frac{g\,\varepsilon}{\tau_0}\,\frac{E_1}{E_i}\,e^{-t/\tau_0}, \quad \ldots\ldots \quad (1)$$

where τ_0 represents the time constant of the decay of the intensity of a scintillation [3]). The fraction E_1/E_i is equal to N, i.e. to the number of electrons liberated from the photocathode that arrive in the dynode system [4]).

This current pulse produces across the anode impedance, consisting of the resistance R_a and the (stray) capacitance C_a in parallel, a voltage pulse of the form:

$$V'(t) = \frac{g\,\varepsilon}{C_a}\,\frac{E_1}{E_i}\,\frac{\tau_1}{\tau_0 - \tau_1}\left\{e^{-t/\tau_0} - e^{-t/\tau_1}\right\}, \quad \ldots \quad (2)$$

where $\tau_1 = R_a C_a$. The peak value of V', i.e. the pulse height, is:

$$V_m' = \frac{g\,\varepsilon}{C_a}\,\frac{E_1}{E_i}\left(\frac{\tau_1}{\tau_0}\right)^{\frac{\tau_0}{\tau_0-\tau_1}}. \quad \ldots\ldots \quad (3)$$

This peak value, even with given E_i and g, is evidently not a fixed quantity. An increase in τ_1/τ_0 causes an increase in V_m': for large τ_1/τ_0 the term in τ_0 and τ_1 approaches the value 1, but the pulse duration is then very long, and this is undesirable having regard to the dead time. *Fig. 1* shows the shape of the pulse for various values of τ_1/τ_0. The pulse shapes at the amplifier output are modified by the frequency response of the amplifier connected to the photomultiplier tube. We shall return to this point in the next section.

The noise

The noise, it will be recalled, consists chiefly of pulses arising from the thermionic emission of electrons from the photocathode in the multiplier tube (mono-electronic pulses). They occur at the rate of some thousands to tens of thousands per second. In addition there is a much smaller number of poly-electronic pulses, which are presumably due to the collision of residual-gas ions against the photocathode. These pulses together constitue what is termed the *dark current* of the multiplier tube.

The mono-electronic voltage pulses are of the form:

$$V_r'(t) = \frac{g'\,\varepsilon}{C_a}\,e^{-t/\tau_1}. \quad \ldots\ldots \quad (4)$$

This formula closely resembles that for the scintillation pulses (2), except that it does not, of course, contain τ_0 and that the number of electrons leaving the photocathode per event is here generally equal to unity (for scintillations this number is equal to E_1/E_i; see (2)). The quantity g' is the amplification factor of the multiplier tube, the value of which fluctuates considerably for mono-electronic pulses. The average value of g' is equal to that of the quantity g found in the formulae (1) to (3). The height of the pulse is $g'\varepsilon/C_a$. Owing to the fluctuation of g', this height differs from one pulse to another; the noise shows a relatively broad pulse-height spectrum.

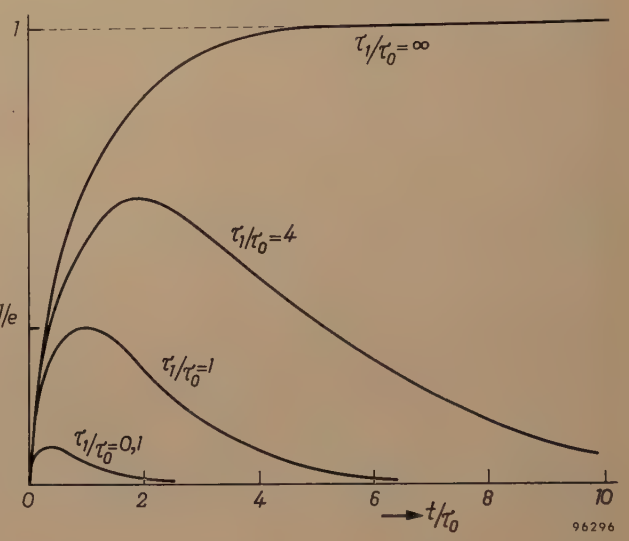

Fig. 1. The shape of scintillation pulses showing their dependence on the ratio between the time constant of the anode circuit of the photomultiplier tube (τ_1) and the decay constant of the scintillation (τ_0). $V'(t)$ (see formula (2)) is plotted on the ordinate (the scale being such that the pulse height is equal to unity for $\tau_1/\tau_0 = \infty$); the abscissa represents the time (in units of τ_0). τ_1/τ_0 must be neither very large nor very small; if it is very large the pulses are too long, while if it is very small difficulties arise which are explained later in this article.

The discriminator level V_{d_1} at which, on an average, one noise pulse is passed per second, depends of course on the form of the noise spectrum — which we shall assume to be constant for all cases — and on I_{th}, the number of thermal noise pulses per second [5]). In the formula

$$V_{d_1}' = \frac{g\,\varepsilon}{C_a}\,D\,(I_{th}) \quad \ldots\ldots \quad (5)$$

the function $D(I_{th})$ describes the influence which the *form* of the noise spectrum and the *intensity* of the noise exert on V_{d_1}'.

[3]) Cf. formula (3) in I. For NaI(Tl) the value of τ_0 is 0.25 μsec.

[4]) The fact that this number differs slightly from pulse to pulse, even with constant E_1, can be disregarded here. The same applies to the fluctuation of g, at least as far as the scintillation pulses are concerned.

[5]) The choice of one noise pulse per second is, of course, somewhat arbitrary. Further details regarding the form of the noise spectrum are given in I and in the appendix to this article.

Scintillation pulses and noise at the amplifier output

If the frequency response of the amplifier were horizontal over the whole frequency range concerned, it would be a simple matter to determine from formulae (3), (4) and (5) the height of the scintillation and noise pulses at the output of the pulse amplifier, as well as the discriminator level at which exactly one noise pulse is counted per second. In that case it would be sufficient merely to multiply these formulae by a constant factor G, the amplification factor. However, in reality the amplifier response is not everywhere horizontal. We shall describe the actual situation by multiplying the factor G by a function φ, which comprises not only the influence of the time constants governing the frequency response of the amplifier but also the effect of τ_1 (the time constant of the anode circuit of the multiplier tube) and τ_0 (the decay constant of the scintillation). This function thus includes all time constants that govern the amplitude of the pulse. The form assumed by φ for scintillation pulses therefore differs from that for noise pulses, since as regards the latter, τ_0 is of no significance: we shall denote the two forms of φ by φ_1 and φ_2 respectively.

Formulae (3) and (5) thus become:

$$V_m = \frac{G g \varepsilon}{C_a} \frac{E_1}{E_i} \varphi_1 \quad . \quad . \quad . \quad . \quad . \quad (6)$$

for the height of the scintillation pulses, and

$$V_{d1} = \frac{G g \varepsilon}{C_a} \varphi_2 D(I_{th}) \quad . \quad . \quad . \quad . \quad (7)$$

for the earlier specified discriminator level.

Let E_{eq} be the value of E_1 at which V_m is equal to V_{d1}. From (6) and (7) we then obtain:

$$E_{eq} = E_i D(I_{th}) \varphi_2/\varphi_1 . \quad . \quad . \quad . \quad . \quad (8)$$

The value of E_{eq} — i.e. the energy of the γ-quanta which, in the case of complete absorption ($E_1 = E_0$), give rise to pulses of a height equal to V_{d1} — is a measure of the signal-to-noise ratio. This ratio is equal to E_0/E_{eq} and hence inversely proportional to E_{eq}.

The effects of E_i, of the thermionic emission and of the time constants on the value of E_{eq} appear separately in eq. (8) [6]). We see that, apart from aiming at low values of E_i and $D(I_{th})$ — as we already know — we must aim at a minimum for φ_2/φ_1.

[6]) The separation of the influences of the dark current and the time constants, as done here, is possible only when the average interval between two pulses (i.e. $1/I_{th}$) is large with respect to the time constants τ_n which determine the pulse duration; in other words, the dimensionless products $I_{th}\tau_n$ must be small. If this is not the case, E_{eq} depends on the values of these products and is larger than follows from eq. (8).

Since the time constants influence not only E_{eq} — and hence the signal-to-noise ratio — but also the dead time of the apparatus, we shall deal with both aspects together in the next section.

Before doing so, however, we must examine rather more closely the nature of φ_1 and φ_2. For this purpose it is necessary to make a certain assumption regarding the frequency response of the pulse amplifier. We shall assume that this has approximately the same shape as the frequency response of the "integrating" network of time constant τ_2, shown on the right of the equivalent circuit in *fig. 2*. The caption to this figure explains the other elements of this diagram, the composition of which is based solely on the mathematical analogy and does not, of course, resemble the actual circuit. For frequencies $f > 1/2\pi\tau_2$ the gain of this network is more than 3 dB smaller than at very low frequencies. Since in our model the lower limit of the range of frequencies passed by the amplifier lies at 0 c/s, the bandwidth of the amplifier is also equal to $1/2\pi\tau_2$.

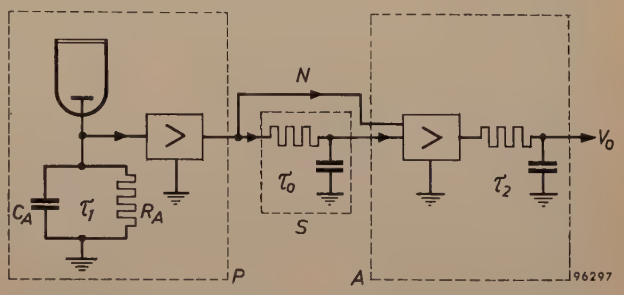

Fig. 2. Equivalent circuit of the counting system: scintillator (S), photomultiplier tube plus anode network (P) and pulse amplifier (A). The two first elements have time constants τ_0 and τ_1, respectively. The frequency response of the amplifier is approximately represented by that of an integrating network of time constant τ_2. The sign $>$ denotes amplification independent of the frequency. The noise is introduced via a separate network N in parallel with S (see formula (4)). The diagram can be justified as follows. Omission of A gives a circuit corresponding to formula (2) for the scintillation pulses at the amplifier input. If S is also omitted, the remainder of the circuit corresponds to formula (4) for the noise pulses.

The form of the functions φ_1 and φ_2

Starting from the assumptions made above, it is possible to write formulae for the scintillation and noise pulses as a function of time. For the scintillation pulses we can write:

$$V(t) = A_1 e^{-t/\tau_0} + A_2 e^{-t/\tau_1} + A_3 e^{-t/\tau_2}, \quad . \quad . \quad (9)$$

and for the noise pulses

$$V_r(t) = B_1 e^{-t/\tau_1} + B_2 e^{-t/\tau_2}. \quad . \quad . \quad . \quad (10)$$

In principle one should be able to find the functions φ_1 and φ_2 by deriving expressions for the height of both types of pulse from (9) and (10). This is

analytically possible for the noise pulses, which are described by only two exponential terms, but not for the scintillation pulses. The way in which φ_1 varies with the different time constants can be found only by numerical calculation. It can, however, be shown that the value of φ_1 — like that of φ_2 — depends solely on the value of the ratios τ_1/τ_0 and τ_2/τ_0. We shall henceforth denote these ratios τ_1' and τ_2', respectively.

It is convenient to represent the numerical results graphically by drawing lines of constant φ in a figure having τ_1' and τ_2' as the coordinates. These lines are thus the loci of all combinations (τ_1', τ_2') leading to the same value of φ. The φ_1 lines were calculated with an electronic computer [7]). *Fig. 3* shows the curves for $\varphi_1 = 0.10$, 0.20, 0.25, 0.30 and 0.368. It is easier to calculate φ_2, since it does not depend on τ_0. A glance at the equivalent circuit of fig. 2 shows that τ_0 and τ_2 play completely analogous parts, that is to say φ_2 depends on τ_1 and τ_2 in the same way as V_m' on τ_1 and τ_0; see formula (3). Just as V_m' was there determined by the ratio τ_1/τ_0, in this case φ_2 is determined by the ratio τ_1/τ_2 (which is equal to τ_1'/τ_2'); in other words, the lines of constant φ_2 in fig. 3 are straight lines through the origin. For large τ_1' and τ_2' the curves $\varphi_1 = \text{const.}$ approach asymptotically the straight lines $\varphi_2 = \text{const.}$ corresponding to the same value of φ_2 (i.e. $\varphi_1 = \varphi_2$).

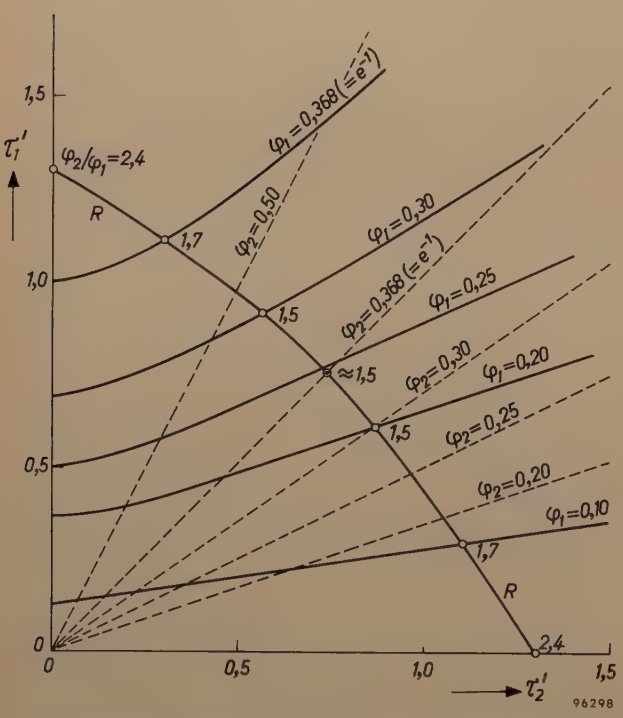

Fig. 3. Graphical determination of the time constants τ_1' and τ_2' with the object of obtaining the most favourable signal-to-noise ratio. With τ_2' on the abscissa and τ_1' on the ordinate, lines of constant φ_1 and φ_2 are drawn (cf. formulae (6) and (7)) from which the value of φ_2/φ_1 can be calculated for any combinaton of τ' values. The lines of constant φ_2 are straight lines through the origin; for large coordinate values each line corresponding to a certain value of φ_1 approaches asymptotically the line of constant φ_2 for which $\varphi_2 = \varphi_1$. Lines of constant pulse duration can also be drawn, e.g. the curve R in the figure refers to a pulse duration of $10\tau_0$. The smallest value of φ_2/φ_1, and hence the most favourable signal-to-noise ratio, is found at points $\tau_1' = \tau_2'$.

[7]) The programming of these calculations was done by A. J. W. Duijvestijn.

Signal-to-noise ratio and dead time as a function of φ_1 and φ_2; bandwidth of pulse amplifier

In every point of fig. 3, i.e. for every combination (τ_1', τ_2'), we now know the values of φ_1 and φ_2 and hence also the value of the ratio φ_2/φ_1. (The latter is always greater than unity.) The problem of the most favourable signal-to-noise ratio can therefore very simply be solved by ascertaining the point of the (τ_1', τ_2') field at which the ratio φ_2/φ_1 is minimum (cf. formula (8)).

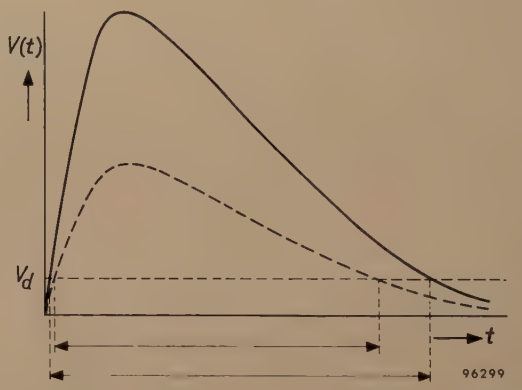

Fig. 4. The pulse duration, i.e. the time during which $V(t)$ is greater than the discriminator level V_d, is not constant but depends on the pulse height.

At the same time, however, the designer must ascertain whether in this case the pulse duration, hence the dead time, also has an acceptable value, and if not, how the time constants must be chosen in order to reach the most favourable compromise.

The pulse duration, which we define for the output pulses as the time during which $V(t)$ is greater than the discriminator level V_d, depends on the form of the pulse, i.e. on all time constants and also on the height of the pulse; see *fig. 4*. Since the dead time of a counter should be constant — a varying dead time would make it impossible in the case of high counting rates to apply a correction for the uncounted pulses [8]) — it may not be determined by the pulse duration. The dead time must accordingly be made at least equal to the maximum possible

[8]) See e.g. Philips tech. Rev. **16**, 360-370, 1954/55 or **17**, 206-221, 1955/56.

value of the pulse duration, i.e. to the duration of the largest pulses [9]). This is done by appropriately designing the electronic circuit of the counter. By "pulse duration" in the following we shall be referring to this maximum value.

At a given τ_0, more than one combination τ_1', τ_2' can lead to a certain pulse duration. The locus of all combinations τ_1', τ_2' leading to the same pulse duration is found to be a curve that is roughly a quadrant about the origin (see fig. 3). It can be shown that this curve (with the same scale of abscissa and ordinate) is symmetrical with respect to the line $\tau_1' = \tau_2'$ (the "diagonal"). The same applies to the variation of φ_2/φ_1 on this curve; the minimum is always on the diagonal. The most favourable solution is therefore to choose $\tau_1' = \tau_2'$. The requisite numerical value of the time constants then depends only on the desired pulse duration.

The curve of constant pulse duration drawn in fig. 3 applies to a pulse duration as defined above, of $10\tau_0$. It can be seen that in this case the minimum value of φ_2/φ_1 is approximately 1.5, and that this value increases the more one moves away along this curve from the diagonal. On the coordinate axes the value has risen to 2.4.

Having decided on the pulse duration and the associated values of τ_1' and τ_2' that lead to a minimum value of φ_2/φ_1, we have then also established E_{eq} (see eq. (8)), the bandwidth of the amplifier (since $2\pi f\tau_2 = 1$) and the pulse heights. For the pulse duration selected above, the corresponding values amount to $\varphi_2/\varphi_1 = 1.5$ (i.e. $E_{eq} = 1.5 \times$ the minimum value [10])), $f = 1$ Mc/s and the pulse height is approximately one quarter of the maximum pulse height ($\varphi_1 \approx 0.25$; see eq. (6)).

Although the frequency response of the pulse amplifier is only approximately represented by a fourpole of time constant τ_2 (fig. 2) — a more detailed representation requires more time constants and therefore involves considerable difficulties — one can nevertheless draw the following conclusions:

1) A large bandwidth with respect to $1/2\pi\tau_0$ results in a low signal-to-noise ratio.
2) A small bandwidth with respect to $1/2\pi\tau_0$ results in a long dead time.

These conclusions are soon arrived at when it is realized that a large bandwidth means a small τ_1' and τ_2'. From fig. 3 it can be seen that φ_2/φ_1 is large for small τ_1' and τ_2', hence E_{eq} is large and the signal-to-noise ratio small. On the other hand, when τ_1' and τ_2' are large, φ_2/φ_1 is approximately equal to unity. This implies a particularly good signal-to-noise ratio, but at the same time the pulse duration, and hence the dead time, is very long (cf. fig. 1).

Choice of pulse duration and dead time

The current pulse from the photomultiplier tube consists of a group of mono-electronic pulses originating from the individual photoelectrons. At the beginning of the current pulses these mono-electronic pulses lie very close together, but in the "tail" the average interval between the moments at which they occur becomes increasingly longer.

If the output pulse duration, determined by the time constants of the apparatus, and the dead time are of the order of magnitude of τ_0 (or smaller), some of the mono-electronic pulses are counted separately. These pulses are indistinguishable from the noise pulses, so that by shortening the pulse duration and the dead time we apparently increase the intensity of the noise. In order to count to more than one "noise" pulse per second in this case, we must therefore raise the discriminator level, which means that a larger fraction of the scintillation pulses will not be counted. The choice of the dead time will accordingly rest on a compromise.

By way of illustration, let us see what the situation is when, as in the example earlier discussed, the pulse duration is made equal to $10\tau_0$. From the formula describing the decay of a scintillation [11]), it follows that the number of photoelectrons occurring after the moment $t = 10\tau_0$ is equal to Ne^{-10}. If the γ-energy absorbed in the scintillator is, say, 3 MeV, this number is approximately equal to one (since N is E_1/E_i, hence in this case about 10^4; $e^{-10} \approx 10^{-4}$). Where the dead time of the counter is also about $10\tau_0$ — i.e. about 2.5 μsec in a counter with an NaI(Tl) scintillator — 10000 scintillations can be counted per second without appreciable correction of the dead time. In our example, then, we also have 10000 "tail pulses", that is to say, the noise intensity is about twice as great. This can be corrected by quite a small increase in the discriminator level (see appendix, eq. (11)).

It is evident from the foregoing that the dead time of a scintillation counter is primarily determined by the nature of the scintillating material. Whatever compromise is chosen, the pulse duration will never be shorter than τ_0; on the contrary, it comes out as a rule at 7 to 10 τ_0. This means that the reso-

[9]) In practice these are pulses produced by γ-quanta of about 3 MeV. Since V_{d_1} in modern counters corresponds to an E_{eq} value of 10 keV, these pulses are about 300 times higher than the discriminator level.

[10]) At an E_i value of 450 eV and a $D(I_{th})$ value of 10 (see appendix), E_{eq} in this case is therefore 6.75 keV (eq. 8).

[11]) See formula (3) in I.

lution of scintillation counters fitted with different scintillating materials can be roughly compared and determined by considering the τ_0 value of the materials in question.

The fact that the dead time of a scintillation counter is almost entirely determined by τ_0 is thus due to a pulse being a group of mono-electronic pulses. If the pulse were a continuous phenomenon, so that no trouble would be experienced from the above-mentioned tail pulses, it would be possible to somewhat reduce τ_1' before the signal-to-noise ratio were as high as that with which we are concerned in the present case. This would, of course, entail more amplification (cf. fig. 1).

Appendix: The form of the noise spectrum

Since little is known theoretically about the statistics of secondary emission, i.e. about the nature of the fluctuations of g', it is not possible to calculate the form of the noise spectrum, nor therefore that of the function $D(I_{th})$. This relation can, however, be deduced from experiments, whereby the number of noise pulses passed per second is plotted against the discriminator level V_d for various values of I_{th}. The results of such a measurement are shown in *fig. 5*. The point at which the curves are intersected by the horizontal line corresponding to $I_d = 1$ yield combinations of D and I_{th} from which the function $D(I_{th})$ can be derived. We find

$$D(I_{th}) \approx 0.9 + 1.25 \log I_{th} \quad . \quad . \quad . \quad . \quad (11)$$

For $I_{th} = 10^4$ pulses per second, D is thus approximately 6.

When poly-electronic pulses are present in any appreciable numbers, the value found for D is substantially higher (see the dashed line in fig. 5). The number of such pulses need not even be particularly large to produce such an increase. A measurement of the dark current does not therefore give much indication of the discriminator level necessary in order to limit the noise count rate to a certain figure.

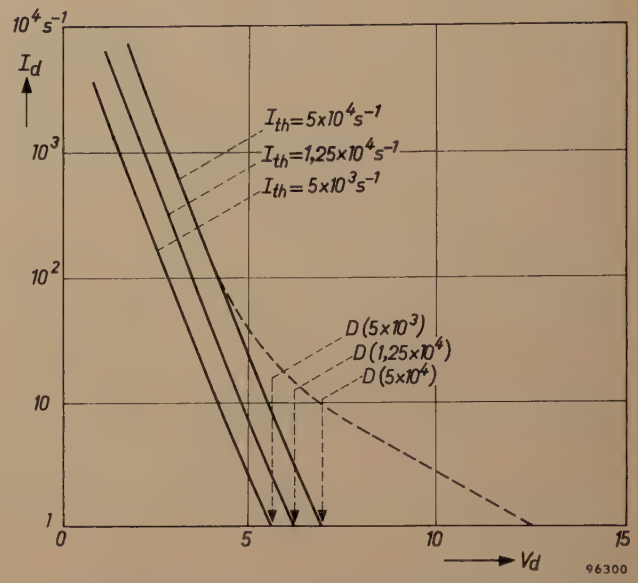

Fig. 5. The relation between the discriminator level at which one noise pulse per second is passed, and the number of (thermionic) noise electrons emitted per second, I_{th}, i.e. the function $D(I_{th})$, can be empirically determined from the points where the horizontal line corresponding to an ordinate value of 1 count per sec intersects the three plotted curves. The latter give the relation between the number of noise pulses passed per second I_d and the discriminator setting V_d, for various values of I_{th}. (The numbers along the V_d axis express the value of V_d in terms of a unit equal to the average noise pulse height.)

Summary. The ratio between the height of scintillation pulses corresponding to a certain absorbed energy and the discriminator level at which no more than (e.g.) one noise pulse per second is counted, the "signal-to-noise" ratio, depends on the decay constant of the scintillation effect (τ_0), on the time constant of the anode circuit of the photomultiplier tube (τ_1) and on the frequency response of the amplifier. If the latter can be approximately represented by only one time constant (τ_2), it is possible to solve, at least numerically, the problem of what combination yields the best signal-to-noise ratio.

The time constants also determine, however, the pulse duration, and hence the dead time of the scintillation counter. The scintillation pulse consists of a group of mono-electronic pulses. To avoid counting too many of these separately in the tail of the scintillation pulse and thereby raising the effective noise level, the pulse duration cannot be made shorter than 7 to 10 τ_0. Having decided on the scintillating material (thus fixing τ_0) and on the pulse duration, one can give the signal-to-noise ratio the largest value possible under these conditions by selecting that combination of τ_1, τ_2 at which $\tau_1 = \tau_2$.

ELECTRON EMISSION OF MATERIALS FOR ELECTRON TUBES

by G. A. ESPERSEN *) and J. W. ROGERS **). 621.385.002:537.581

The characteristics of some electron tubes, especially those operating at high power, are often adversely affected by electron emission from parts of the tube other than the cathode. This unwanted emission depends to a great extent on the material used. Certain components therefore need to be made of materials which, even when hot, emit few electrons. This article describes an investigation of a number of such materials used in the construction of electron tubes.

Introduction

In conventional electron tubes the cathode is always regarded as the sole source of the electron current to the anode. The cathode is made emissive by heating it and the emission density is increased by coating the cathode with a substance possessing a low work function. Emission from other parts [1]) gives a tube characteristics which were not intended by the designer, and as a rule impairs its operation. The parts most likely to be responsible for unwanted thermionic emission are of course those which get very hot during normal duty. This may be expected particularly in high-power tubes, e.g. transmitting tubes. In conventional transmitting tubes the control grid is the worst offender in this respect since, for various reasons, it can acquire a fairly high temperature. The main reasons are:

a) The grid absorbs part of the heat radiated by other electrodes. Naturally the principal source of this heat is the cathode, but the anode is an important source of heat in tubes where the anode is not cooled by air or water.

b) The grid is difficult to cool by conduction.

c) In an operating transmitting tube the grid is generally positive with respect to the cathode for a part of every cycle. During this time the grid is bombarded by electrons from the cathode (i.e. grid current flows), and this bombardment contributes to the heating of the grid.

d) At high frequencies the internal capacitances of the tube generally form part of the circuit capacitances, resulting in appreciable high-frequency currents through the grid wires and hence extra heating.

With regard to grid emission, another unfavourable circumstance is that evaporation products from the cathode can readily collect on the grid surface, thereby substantially lowering its work function. Most important of all, electron emission from the grid has more undesirable effects on the circuit than emission from other electrodes.

Another type of tube in which undesired electron emission may occur are magnetrons. In this case a high temperature and vapour deposits from the cathode on the end caps enclosing the electrode system of the magnetron can also give rise to unwanted thermionic emission.

In the construction of an electron tube two methods are adopted to reduce unwanted emission from certain components:

a) The components are designed and assembled in such a way as to ensure that they are heated as little as possible.

b) The components are made of a material possessing a high work function, even when covered with evaporation products from the cathode [2]).

In connection with the latter point, an investigation was carried out some years ago at Irvington to examine the suitability of various materials for use in the construction of electron tubes [3]). In the present article we shall describe these experiments and the results obtained.

The investigation was made with tubes specially designed for the purpose, and the utmost care was taken to ensure maximum cleanliness of all parts, since even minute contaminations have a very marked effect on the emission characteristics of a material.

Construction and processing of the experimental tubes

For the majority of experiments, tubes of the planar-triode type as represented in *fig. 1* were used.

*) Philips Laboratories, Irvington-on-Hudson, N.Y., U.S.A.
**) Formerly with Philips Laboratories, Irvington.

[1]) Secondary emission, which is usefully employed in some electron tubes, is not considered here.

[2]) A design has been considered whereby the components likely to give rise to unwanted emission become so hot during normal operation that cathode material deposited on them is either absorbed or readily evaporated again. This method, however, is difficult to control.

[3]) See G. A. Espersen and J. W. Rogers, Studies on grid emission, I.R.E. Transactions on Electron Devices **ED 3**, 100-107, 1956.

The anode consisted of a molybdenum cylinder. The cathode had the same dimensions as the anode and was heated by an internal filament. The material under investigation was placed in the form of a loop of 0.010″ wire midway between cathode and anode.

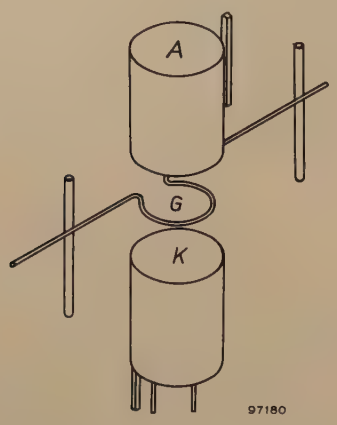

Fig. 1. Schematic representation of the structure of the experimental tubes. *A* anode, *G* "grid", *K* cathode.

The diameter of the loop was 0.085″. Because of its position in the electrode system, we shall refer to this loop henceforth as the "grid". In addition to this structure, a getter and also a diode consisting of a tungsten filament and a molybdenum anode, were incorporated in the envelope. The purpose of the latter was to enable the vacuum in the tube to be checked by measuring the work function of the tungsten filament. A bad vacuum increases the work function. Exclusive use was made of tungsten, molybdenum and tantalum for the tube structure, including the stem leads. The grid consisted of the material to be tested. Before assembly, all components were thoroughly cleaned. Careful precautions were taken during assembly to prevent contamination of the components. For example, to avoid copper deposits during the welding of the electrodes, welding tips of tungsten were employed.

During the sealing-in of the electrodes in the glass envelope, care was taken to avoid excessive heating of the triode structure, by simultaneously passing a stream of dry nitrogen through the envelope. The entire tube was baked for one hour at 720 °K while being evacuated. During the pumping process the parts were degassed by heating in the usual way, the getter being glowed below its flashing temperature. The getter was not flashed until about ten minutes after the tube had been sealed off, during which time the tube was "seasoned" at a high temperature. Immediately before sealing-off, and again about a day later, the vacuum in the tube was checked with the aid of the auxiliary diode. If at that time the vacuum was found to have deteriorated, the tube was rejected.

Two types of triode were used, one being a single-ended structure and the other a double-ended structure with the anode and grid terminals brought out at opposite ends of the envelope. In the latter case the leakage path between anode and grid has a higher resistance, and this type of tube was therefore used when the emission current to be measured was less than about 0.2 mA peak.

Methods of measurement

Most of the measurements were made by a method [4]) in which the grid was heated continuously, either by direct conduction or by electron bombardment. Once every $^1/_{60}$ second a negative voltage pulse of 100 microseconds duration was applied to the grid, each pulse producing a sufficiently large potential difference between the grid and the other electrodes to give rise to grid emission currents of saturation value. A plot of grid current versus time is shown in *fig. 2*. The grid emission was measured by determining the amplitude of the current pulses on an oscilloscope.

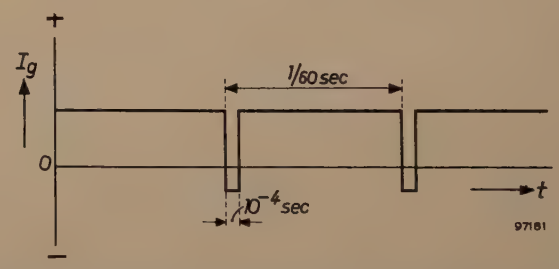

Fig. 2. Grid current I_g versus time t in a grid-emission measurement by the pulse method.

When the emission current was less than about 0.2 mA peak it was necessary to abandon the pulse method because of the sensitivity limitation of the oscilloscope. In such cases a D.C. method was used in which the emission current was measured by a galvanometer, the grid being raised to the required temperature with an auxiliary current (see *fig. 3*). In principle this method is simpler than the pulse measurement. However, it was found desirable to use the D.C. method only when the low value of grid current made it necessary, the reason being that the measurements could be made in a much shorter time by the pulse method, hence with much less chance of the conditions in the tube changing during a test run.

[4]) Developed by R. A. La Plante, Amperex Electronic Company.

The main materials subjected to emission tests were tungsten, molybdenum, gold-plated molybdenum and titanium. Loops were made of these materials as denoted by *G* in fig. 1. Since the extent to which evaporation products collect on these

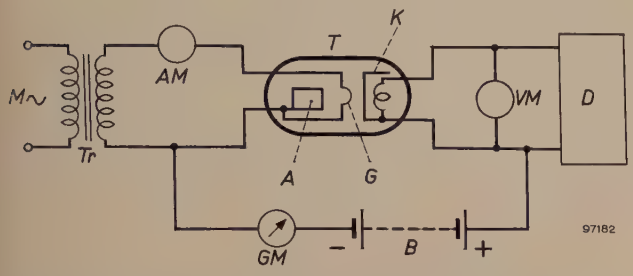

Fig. 3. D.C. method of measuring grid emission. *T* tube under test, *M* mains voltage, *Tr* transformer for heating grid *G*, *D* filament supply, *B* battery, *AM* ammeter, *VM* voltmeter, *GM* galvanometer.

loops depends on the properties of the cathode, three different types of cathode were used in the tubes under test, viz. L cathodes [5]), impregnated cathodes [6]) and oxide cathodes.

Results

During the measurements the L-type and impregnated cathodes were operated at 1275 °K, and the oxide cathodes at 1100 °K, all types having first been run for 100 hours to stabilize their properties. In the course of this "seasoning" the grid remained fairly cold and the evaporation products of the cathode settled in layers on its surface. In many cases these deposits were removed by "glowing" the grid, i.e. by passing a current through it, prior to the measurement. Some measurements were carried out, however, without the grid having first been cleaned after seasoning.

The variation of the grid emission as a function of time is shown for several grid materials in *fig. 4*. In these tests an L cathode was used, operated at 1275 °K. The temperature of the grids was 1200 °K, with the exception of the gold-plated molybdenum grid, which was heated to only 1100 °K, the reason being that above this temperature the gold would evaporate. For the same reason the gold-plated grids, unlike all others, could not be cleaned after seasoning by glowing them as described above.

It appears from fig. 4 that in all cases the grid emission decreases as a function of time and approaches a stable equilibrium value. For tungsten and gold-plated molybdenum, however, the emission

[5]) H. J. Lemmens, M. J. Jansen and R. Loosjes, Philips tech. Rev. **11**, 341-350, 1949/50.
[6]) R. Levi, Philips tech. Rev. **19**, 186-190, 1957/58.

Table I. Final value of the saturation grid emission current for various grid materials when an L cathode operated at 1275 °K was used. (The symbols Mo + Zr or Ca or Mg and Mo + Au indicate molybdenum plated with the second metal; Mn-Ni is an alloy of manganese and nickel.)

Material	Grid temperature (°K)	Grid current (μA)
W	1200	414
Mo	1200	300
Mo+Zr or Ca or Mg	1200	24
Mn-Ni	1200	24
Mo + Au	1100	4.48
Zr	1200	2.24
TiO_2	1200	0.10
Ti	1200	0.0004

rises to a maximum before beginning to drop. The time needed to reach the stable equilibrium value is always short compared with the life of the tube, and in practice therefore it is this final value that is of major importance. The stable equilibrium values for a number of materials are collected in *Table I*. From this table, and also from fig. 4, it can be seen that of all the materials tested, titanium exhibits the lowest emission, both as bright titanium wire and when plated on a core of molybdenum. The emission rises sharply, however, if the titanium is covered with titanium oxide.

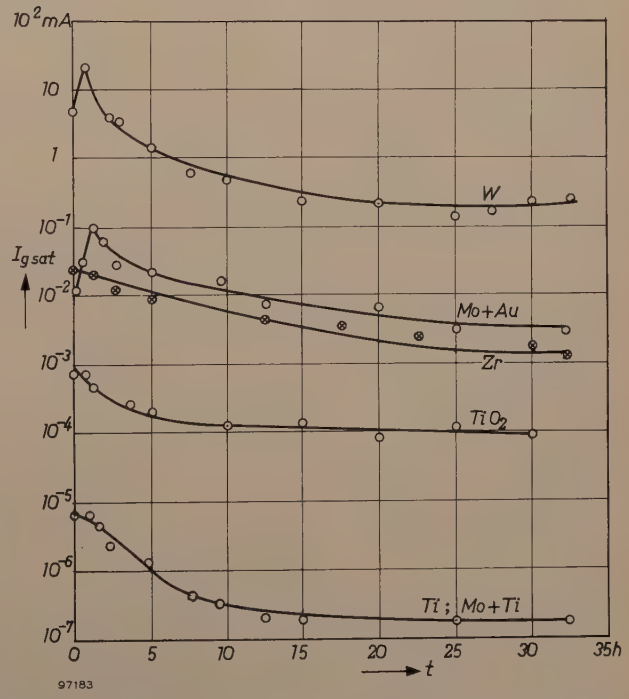

Fig. 4. Saturation grid emission current $I_{g\,sat}$ versus time for various grid materials in an experimental tube fitted with an L cathode. Mo + Au means gold-plated molybdenum, and Mo + Ti titanium-plated molybdenum. Prior to each run the grids, except the Mo + Au grid, were cleaned by heating them for several hours. During the measurements the temperature of the gold-plated grid was 1100 °K and of the others 1200 °K.

To illustrate the influence of the cathode employed, the results are given in *Tables II* and *III* of a series of measurements run with the three types of cathode mentioned above. Table II refers to a tungsten grid and Table III to a gold-plated molybdenum grid. The tables give the initial, maximum and final values of the emission current, together with the time required to reach maximum emission [7]).

Table II. Saturation grid emission current of a tungsten grid at 1200 °K, using three different types of cathode.

Cathode	Cathode temperature (°K)	Grid emission current (mA)			Time required to reach max. value (hours)
		Initial value	Max. value	Final value	
Impregnated	1275	2.0	17	2.6	1.0
L	1275	2.1	50	17	18
Oxide	1100	3.7	54	8.0	25

Table III. Saturation grid emission current of a gold-plated molybdenum grid at 1100 °K, using three different types of cathode.

Cathode	Cathode temperature (°K)	Grid emission current (mA)			Time required to reach max. value (hours)
		Initial value	Max. value	Final value	
Impregnated	1275	0.70	1.1	0.28	2
L	1275	0.21	1.8	0.21	5
Oxide	1100	0.60	2.8	0.21	25

Titanium having been found to have the lowest emission, more comprehensive measurements were carried out on this material [8]). *Fig. 5* shows emission plotted as a function of grid temperature for a grid of pure titanium and for a grid coated with titanium oxide. It is noticeable that oxidation causes a sharp increase in the emission of titanium. At a temperature of 1600 °K the oxide is reduced to titanium and the curve for the oxide therefore falls back to that corresponding to the pure metal. (Experiments performed by V. L. Stout [9]) have shown that the oxygen formed in this process is not liberated but is dissolved in the titanium.)

[7]) The data for the L cathode in Tables II and III are not in agreement with fig. 4. The reason is that the measurements concerned were performed under different conditions. For the data in the tables, the pulsed grid voltage was applied only during the short intervals required for the measurements and not throughout the entire time mentioned in the tables. In the runs whose results are illustrated in fig. 4, the pulsed grid voltage was applied continuously.

[8]) G. A. Espersen, U.S. Patent 2 846 609, 5 August 1958: Non-emissive electrode for electron-discharge device.

[9]) Private communication from Dr. V. L. Stout, General Electric Research Laboratory, Schenectady, N.Y., U.S.A.

In the measurements to which fig. 5 refers, an L cathode was used. After seasoning the cathode at 1500 °K, the evaporation products deposited on the grid were not removed, and this probably explains the remarkable shape of the emission curve for titanium. During the increase of the grid temperature to about 1000 °K, the cathode material deposited on the grid is activated, causing the emission to rise in spite of the fact that above 600 °K there is appreciable evaporation of the barium. With the grid above 1000 °K, however, the deposits on the grid evaporate almost completely, causing a drop in

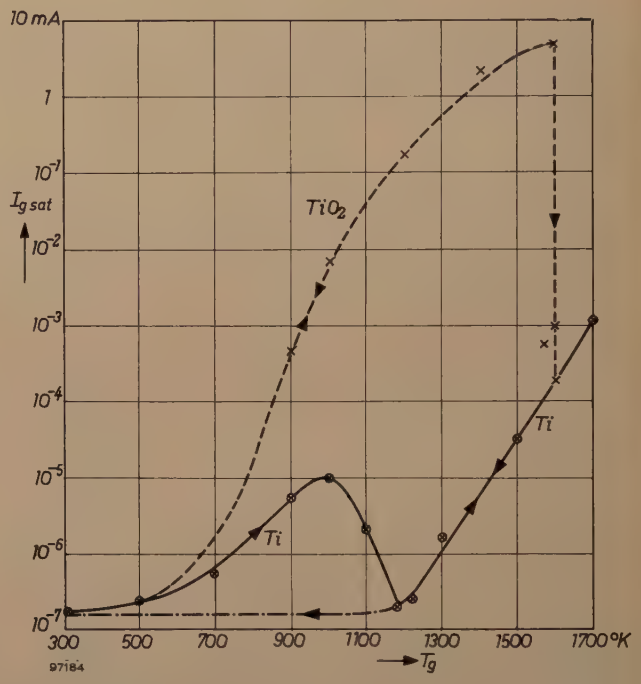

Fig. 5. Saturation grid emission current $I_{g\,sat}$ as a function of grid temperature T_g for bright titanium and for oxidized titanium (tube with L cathode). The cathode evaporation products deposited on the grid were not removed before measurement.

emission, and finally, above 1175 °K, the emission rises again in accordance with the characteristic for pure titanium. This explanation was confirmed by the fact that, when the grid temperature dropped again, the emission underwent no rise below 1175 °K, but showed the values denoted by the dot-dash curve in fig. 5.

The emission from a titanium-plated molybdenum wire was found to be virtually identical with that from a wire consisting entirely of titanium. For molybdenum wire sprayed with titanium powder, however, the emission was several orders of magnitude higher. This was probably due to traces of oxide in the powder used.

Fig. 6 shows how the emission of titanium varies

as a function of time at different temperatures. Prior to these measurements the grid had been exposed for some hours to an L cathode glowing at 1500 °K, during which time it had acquired deposits of cathode material. At the end of each run the grid was cleaned by heating it, after which the cathode was again glowed for some time at 1500 °K. In this way the same conditions were obtained at the beginning of each series of measurements. The

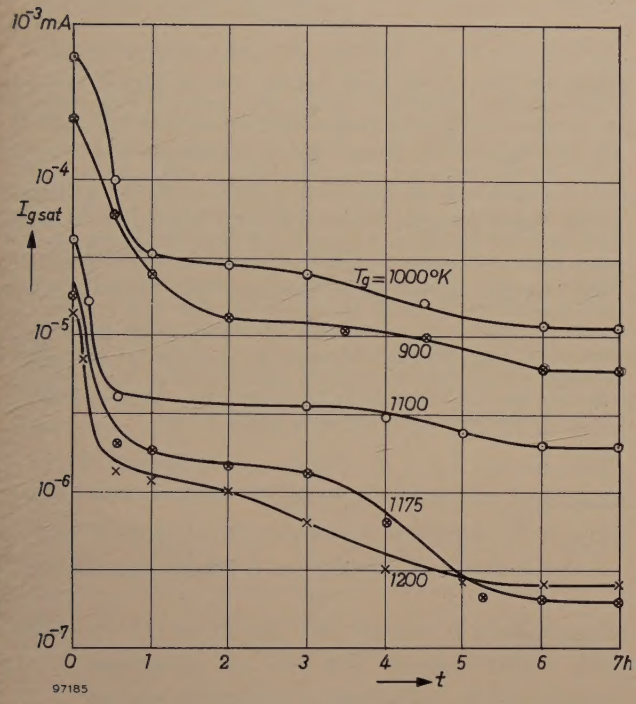

Fig. 6. Saturation grid emission current $I_{g\ sat}$ of titanium grid as a function of time t (hours) for various values of grid temperature T_g (tube with L cathode).

emission characteristic of non-oxidized titanium as a function of temperature, as illustrated in fig. 5, is fully confirmed by the final values indicated by the curves in fig. 6.

Measurements in which evaporation products from the cathode had already settled on the grid beforehand (and were thus not first removed) were also carried out on materials other than titanium. Some results are represented in *fig. 7*, together with the curve for titanium already given in fig. 5. The grid emission characteristics of zirconium and tungsten also show dips. They occur at 1600 °K and 1900 °K, respectively (the latter dip falls outside the figure). The dip is not as great for these materials as for titanium, however. Again, the reason for these minima is believed to be the reduction of barium oxide to barium, which is evaporated from the surface of the grid while the oxygen dissolves in the base material [10]).

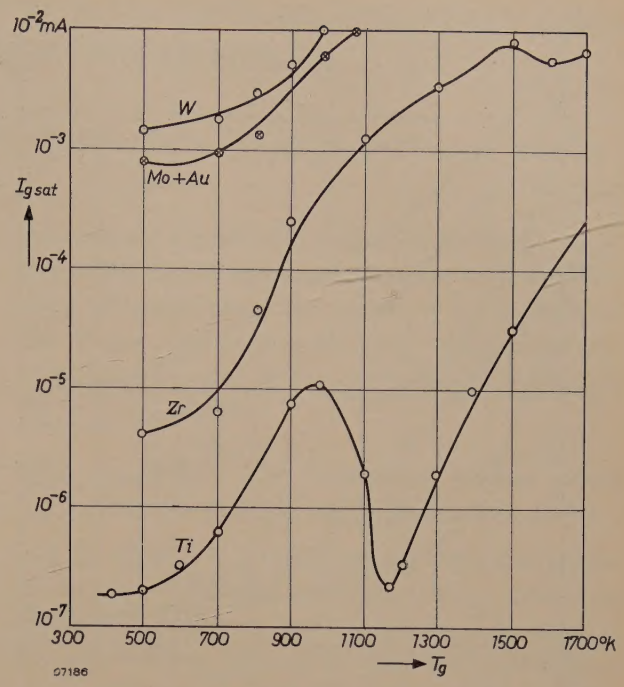

Fig. 7. Saturation grid emission current $I_{g\ sat}$ as a function of grid temperature T_g for various grid materials (tube with L cathode). The cathode evaporation products deposited on the grid were not removed prior to the measurement.

In order to ascertain the rate at which the cathode material deposited on the grid evaporates when it is not continuously supplemented by further evaporation products from the cathode, measurements were carried out with the L cathode kept cold. Prior to each run the grid was exposed, as before, to the evaporation products of the cathode which was glowed at 1500 °K. The results of these measurements for several materials are set out in *Table IV*.

Table IV. Decay of grid emission current for grids of various materials covered with evaporation products of an L cathode. During the measurements the cathode was not heated. (Mo + Au denotes gold-plated molybdenum.)

Grid material	Grid current (mA)		Time required to reach final value (hours)
	Initial value	Final value	
W	39	1.7	28
Mo + Au	9.6×10^{-3}	3×10^{-3}	10
Zr	5.4×10^{-3}	2.2×10^{-3}	6
Ti	0.6×10^{-3}	0.3×10^{-3}	7
TiO_2	2×10^{-3}	0.058×10^{-3}	—

The values tabulated are the initial and final values of the emission current, and the time needed to reach approximately the final value. During the measurements the grid temperature was 1200 °K,

[10]) X-ray diffraction analyses were made to determine whether the barium combined with the titanium instead of evaporating. No titanates were found.

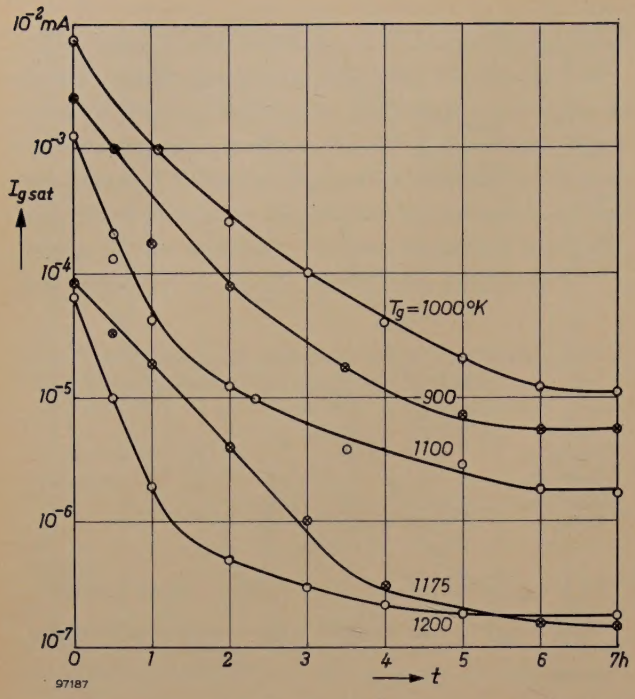

Fig. 8. Saturation grid emission current $I_{g\,sat}$ of titanium grid as a function of time t (hours) for various values of grid temperature T_g. During the measurement the cathode was kept cold.

with the exception of the gold-plated molybdenum grid which, for the reasons already given, was heated to only 1100 °K. For titanium the measurements were repeated at various other temperatures. The results of these tests are represented in *fig. 8*. Prior to each run the grid was exposed for 16 hours to the cathode at 1500 °K, so that the starting conditions can again be regarded as equal for all curves. From fig. 8 it can be seen that in all cases the cathode deposits on the grid have evaporated after a few hours.

Summary. The operation of certain types of vacuum tube is often seriously affected by thermionic emission from parts of the tube exposed to the evaporation products of the cathode. The extent to which this unwanted emission occurs depends partly on the materials used. With this in mind, an investigation was made into the emissive properties of various materials widely used in the construction of electron tubes. Special tubes were built for this purpose, care being taken to ensure that all parts were scrupulously clean. To simulate practical operating conditions, the cathode evaporation products were allowed to form deposits on the grid. Measurements were also carried out at different operating temperatures. Three types of cathode were used, viz. impregnated cathodes, L cathodes and oxide cathodes. Of all materials tested, clean titanium was found to have the lowest emission. It shows a much greater emission, however, if coated with titanium oxide.

ABSTRACTS OF RECENT SCIENTIFIC PUBLICATIONS BY THE STAFF OF N.V. PHILIPS' GLOEILAMPENFABRIEKEN

Reprints of these papers not marked with an asterisk * can be obtained free of charge upon application to Philips Electrical Ltd., Century House, Shaftesbury Avenue, London W.C. 2.

2598: T. J. de Man, J. R. Roborgh and E. J. ten Ham: Effect of the method of administering massive doses of vitamin A on the liver storage in rats (T. Diergeneesk. **83**, 380-387, 1958, No. 10).

Experiments with rats showed a better liver storage of vitamin A when this vitamin was given orally as a massive dose from an aqueous dispersion than when applied in the same way from an oily solution. Only a very small percentage of the vitamin A from an oily solution, administered intramuscularly, was stored while under the same conditions from an aqueous dispersion about 60% could be recovered in the liver. The liver storage from an aqueous dispersion of vitamin A, given intravenously, proved to be about 70% of the applied dose. The vitamin A content of a liver depot in rats decreased but slowly in 1-1.5 month, indicating that a liver depot of a sufficiently high level is able to supply the necessary amounts of vitamin A to the animal for a considerable length of time.

2599: F. W. de Vrijer: The choice of chrominance signals in the N.T.S.C. system with a view to the differential sensitivity of the human eye to colour (Acta electronica **2**, 103-109, 1957/58, No. 1/2).

In an N.T.S.C.-type colour-television system the phase of the subcarrier determines to a first approximation the hue, and the amplitude of the subcarrier relative to the value of the luminance signal determines the saturation of the reproduced colour in a colour-receiver. Colour deviations will occur in case of noise in the chrominance channel and in case of phase errors of the receiver subcarrier reference oscillator. These phase errors may be caused by noise or otherwise. The sensitivity of the signal to these effects is influenced by the particular choice of chrominance signals transmitted. In order to make an optimum choice, the differential sensitivity of the human eye to colour has to be taken into account. In this paper known data on hue tolerances are used to calculate the sensitivity to phase errors in the N.T.S.C. system. Experiments were performed with an actual colour-television system to get more exact numerical data. These data are used to calculate the optimum choice of chrominance signals with respect to subcarrier phase errors. This optimum choice turns out to be not very much different from the actual N.T.S.C. system. The paper concludes with some remarks on the sensitivity to noise in the chrominance channel of the N.T.S.C. signal.

2600: L. Heijne: The lead-oxide vidicon (Acta electronica **2**, 124-131, 1957/58, No. 1/2).

A description is given of an experimental photoconductive television pick-up tube, using an evaporated layer of lead monoxide. The layer is microcrystalline. The most important properties of the tube are: *a*) negligible dark current (approx. 0.003 μA); *b*) high sensitivity (100-200 μA/lm); *c*) approximately linear light-transfer characteristic; *d*) fast response also at low light levels. The sensitivity is maximum in the blue or green parts of the spectrum depending on the thickness of the photoconductive layer. The decay of the signal after a sudden interruption of the light is primarily determined by the discharging mechanism of the scanning beam, and not by inherent inertia of the photoconductor itself. At high illumination levels the photocurrent may become saturated as a result of progressive target discharge. At short wavelengths space-charge in the interior of the photoconductor may also limit the signal current. The influence of target thickness on decay, gamma and spectral response is discussed in detail.

2601: H. A. Klasens and A. Bril: Phosphors for colour television (Acta electronica **2**, 143-152, 1957/58, No. 1/2).

When selecting the most suitable phosphors for tricolour tubes and projection tubes for colour television, the following points have to be considered: *a*) The colour reproduction. *b*) The overall efficiency. *c*) The picture quality. To obtain the best colour reproduction, the chromaticity coordinates should be as near as possible to the corners of the chromaticity diagram. For the calculation of the lumen output of the screen a white colour with chromaticities $x = 0.310$ and $y = 0.316$ (illuminant C) was chosen, since most objects have rather unsaturated colours. It is shown that the choice of the red phosphor mainly determines the luminous properties of

the screen and that a compromise has to be found between colour reproduction and light output. The ideal red phosphor should have a narrow emission band with a sharp cut-off towards shorter wavelengths near 6100 Å. Stray electrons and misalignment of the primary electron beam cause some colour distortion and loss of contrast in tricolour tubes. The picture quality can be improved by reducing the efficiencies of the green and blue phosphors. Such a phosphor compensation may furthermore improve the gamma match in three-gun tubes. Phosphors for flying-spot tubes are briefly discussed.

2602: J. C. Francken and R. R. Bathelt: Measurement and evaluation of colour purity in colour tubes (Acta electronica **2**, 153-158, 1957/58, No. 1/2).

Purity of the separate colour fields in colour tubes is one of the requirements for achieving good colour rendition. After a short survey of possible causes of deterioration of the primary colour and of the known methods for measuring chromaticity, a colorimeter is described, especially designed for use with colour tubes. The instrument is based on the principle of visual additive mixing of three light sources. As such three special cathode-ray tubes are used, fitted with the same phosphors as are used in colour tubes. A rapid evaluation of colour purity is thus possible, as well as a quantitative computation of chromaticity coordinates. The accuracy of the method is greatest in the vicinity of the primaries, a property that suits the purpose. Examples of measurements on actual tubes are given. For routine testing of tubes, in cases where reject limits have already been established, an objective method using coloured filters in combination with a photomultiplier is easier and faster. A short description is given of the combinations used for colour-tube testing.

2603: E. F. de Haan and H. Zimmer: Postfocussing colour tubes (Acta electronica **2**, 189-193, 1957/58, No. 1/2).

A colour tube, using a focussing mask, is discussed. The holes in the mask are slits of a special form in order to obtain postfocussing action with a low voltage ratio between mask and screen. A transparency of 60% has been obtained for the mask. It is found that a spherical mask with these slits is easy to construct and therefore it is possible to use a normal envelope with a spherical inner face. Moreover, it is possible to deposit the phosphors by the married-parts method. The phosphor lines have a critical determined width in order to obtain better contrast.

2604: J. Haantjes: Physical aspects of coding systems used in colour television (Acta electronica **2**, 320-326, 1957/58, No. 1/2).

This paper deals with several physical and physiological phenomena playing a role in the viewing of television images. The influence of these phenomena in the choice of an appropriate signal carrying the essential information in an effective way is discussed. This problem cannot yet be considered as completely solved as it still forms the subject of many investigations. The choice of an adequate colour-television system raises again problems of the same nature. The properties of the human eye with regard to the observation of colour and colour detail are dealt with. Besides factors of a physical nature other factors of technical and economic importance have to be taken into account in the choice of a colour transmission system. After discussion of some proposed methods the opinion is expressed that under the circumstances a system on the principle of that adopted in the U.S.A could also be introduced in Europe. The paper ends with a report of the work done in the Philips Research Laboratory at Eindhoven with regard to the adaptation of the N.T.S.C. system to the existing 625 line monochrome standard.

2605: J. E. Rombouts and A. Kaars Sijpesteijn: The chemotherapeutic effect of pyridine-2-thiol-*N*-oxide and some of its derivatives on certain plant diseases (Ann. appl. Biol. **46**, 30-36, 1958, No. 1).

Limited systemic protection of broad bean against *Botrytis fabae* and of cucumber against *Cladosporium cucumerinum* has been observed as a result of the application of pyridine-2-thiol-*N*-oxide and its carboxymethyl derivative. Apparently this protection is, to some extent, the result of translocation of the chemicals in the plants. It was found that the vapour phase of pyridine-2-thiol-*N*-oxide plays an additional role in the chemotherapeutic activity. There is no evidence that the copper chelate of pyridine-2-thiol-*N*-oxide is translocatable in plants. Root applications of these three compounds had no chemotherapeutic effect.

2606: C. J. Bouwkamp: A simple method of calculating electrostatic capacity (Physica **24**, 538-542, 1958, No. 6).

Attention is drawn to a simple theorem enabling the evaluation of the electrostatic capacity of certain conductors in free space such as a system of two spheres in contact with each other and a "ring without hole".